2012-01-09

Biomechanical Implications of Lumbar Spinal Ligament TransectionA Finite Element Study

Gregory Allen Von Forell
Brigham Young University - Provo

Biomechanical Implications of Lumbar Spinal Ligament Transection

A Finite Element Study

Gregory A. Von Forell

A thesis submitted to the faculty of
Brigham Young University
in partial fulfillment of the requirements for the degree of

Master of Science

Anton E. Bowden, Chair
Larry L. Howell
Steven E. Benzley

Department of Mechanical Engineering

Brigham Young University

April 2012

ABSTRACT

Biomechanical Implications of Lumbar Spinal Ligament Transection
A Finite Element Study

Gregory A. Von Forell
Department of Mechanical Engineering, BYU
Master of Science

The purpose of this work was to determine the possible effects of isolated spinal ligament transection on the biomechanics of the lumbar spine. A finite element model of a lumbar spine was developed and validated against experimental data. The model was tested in the primary modes of spinal motion in the intact condition, followed by comparative analysis of isolated removal of each spinal ligament. Results showed that stress increased in the remaining ligaments once a ligament was removed, potentially leading to ligament damage. Results also showed changes in bone remodeling "stimulus" which could lead to changes in bone density. Isolated ligament transection had little effect on intervertebral disc pressures. All major biomechanical changes occurred at the same spinal level as the transected ligament, with minor changes at adjacent levels. The results of this work demonstrate that iatrogenic damage of spinal ligaments disturbs the load sharing within spinal-ligament complex and may induce significant clinical changes in the spinal motion segment.

Keywords: Gregory Von Forell, lumbar, spine, finite element analysis, ligament, biomechanics, spinal surgery

ACKNOWLEDGEMENTS

I would like to thank my committee members, Dr. Benzley and Dr. Howell. Special thanks go to my advisor Dr. Bowden, not only for giving me the much needed guidance and direction, but also for inspiring me to remember that our real purpose in BABEL is to help people live healthier, happier lives. I want to thank every member of BABEL who assisted me in my work, especially the members of the numerical analysis team who spent countless hours with me on the model. I appreciate the funding received from the National Science Foundation (Grant No. 0952758). I am also so very grateful for everything that my wife Stephanie did and does for me.

TABLE OF CONTENTS

LIST OF TABLES ..... **vii**
LIST OF FIGURES ..... **ix**
1. INTRODUCTION 1
1.1 Problem Statement 1
1.2 Summary 2
2. LIGAMENT BACKGROUND 3
2.1. Lower Back Pain 3
2.2. Lumbar Spine Anatomy 3
2.2.1 Locations of Ligaments 6
2.2.2 Ligament Material Properties 7
2.3. Spine Surgery 9
3. FINITE ELEMENT ANALYSIS BACKGROUND 11
3.1. Introduction to Finite Element Analysis 11
3.2. Current Efforts to Model the Spine 12
3.3. Structures 13
3.3.1 Vertebrae 14
3.3.2 Disc 16
3.3.3 Muscles 17
3.3.4 Ligaments 18
3.4. Mesh 19
3.5. Contact 22
3.6. Loading 22
3.7. Validation 23
4. IMPLICATIONS OF SPINAL LIGAMENT TRANSECTION 29
4.1. Introduction 29
4.2. Methods and Materials 31
4.2.1 Finite Element Model 31

4.2.2 Verification and Validation 34
4.2.3 Simulated Testing Procedure 35
4.3. Results 35
4.4. Discussion 40
5. ADDITIONAL INSIGHT 43
5.1 Additional Results 43
5.2 Additional Discussion 47
6. SUMMARY AND FUTURE WORK 49
6.1 Summary 49
6.2 Future Work 49
REFERENCES 51
APPENDIX A. DISC PRESSURE RESULTS 57
APPENDIX B. LOAD SHARING RESULTS 61
APPENDIX C. LOADING FILES 73
C.1 Loading 73
C.2 Materials 75
C.2.1 Rigid Bodies 75
C.2.2 Vertebrae 75
C.2.3 Intervertebral Discs 76
C.2.4 Ligaments 76
C.2.5 Follower Load 77
C.3 Supercomputer 77

LIST OF TABLES

Table 3-1: Cortical Maximum Pricipal Strains (Microstrain) 26
Table 4-1: Material Formulations and Properties 32
Table 4-2: Ligament Properties 34
Table B-1: Normal Load Forces in First Axial Rotation 61
Table B-2: Normal Load Forces in Second Axial Rotation 60
Table B-3: Normal Load Forces in Extension 61
Table B-4: Normal Load Forces in Flexion 62
Table B-5: Normal Load Forces in First Lateral Bending 63
Table B-6: Normal Load Forces in Second Lateral Bending 64
Table B-7: Transverse Load Forces in First Axial Rotation 65
Table B-8: Transverse Load Forces in Second Axial Rotation 68
Table B-9: Transverse Load Forces in Extension 69
Table B-10: Transverse Load Forces in Flexion 70
Table B-11: Transverse Load Forces in First Lateral Bending 71
Table B-12: Transverse Load Forces in Second Lateral Bending 70

LIST OF FIGURES

Figure 2-1: Vertebral Body Numbering 4
Figure 2-2: Vertebra 5
Figure 2-3: Location of Ligaments 6
Figure 2-4: Ligament Stress-Strain Curve 8
Figure 3-1: Intervertebral Disc Geometry 17
Figure 3-2: Parts for Vertebrae Meshing 20
Figure 3-3: Mesh and Double Mesh for Stress Convergence 21
Figure 3-4: Element Jacobians 21
Figure 3-5: Loading Directions 23
Figure 3-6: Motion Validation 21
Figure 3-7: Disc Pressure Data Frei et al. (2001) Spine. 23
Figure 3-8: Disc Pressure During Compression 21
Figure 3-9: Location of Axes of Rotation Pearcy and Bogduk, (1998), Spine 23
Figure 3-10: Location of Axes of Rotation in Current Model 21
Figure 4-1: Hexahedral Finite Element Model of the Lumbar Spine 31
Figure 4-2: Ligament Stress Changes 36
Figure 4-3: Stress Contours During Flexion 37
Figure 4-4: Intervertebral Disc Pressure 38
Figure 4-5: Change in Remodeling Stimulus 39
Figure 5-1: Change in Range of Motion 43
Figure 5-2: Pedicle Stress During First Axial Rotation 44
Figure 5-3: Pedicle Stress During Second Axial Rotation 44
Figure 5-4: Pedicle Stress During Extension 45
Figure 5-5: Pedicle Stress During Flexion 45
Figure 5-6: Pedicle Stress During First Lateral Bending 46
Figure 5-7: Pedicle Stress During Second Lateral Bending 46
Figure 5-8: Normal Load Sharing Between L3 and L4 47
Figure A-1: Disc Pressure During First Axial Rotation 57
Figure A-2: Disc Pressure During Second Axial Rotation 57
Figure A-3: Disc Pressure During Extension 58
Figure A-4: Disc Pressure During Flexion 58
Figure A-5: Disc Pressure During First Lateral Bending 59
Figure A-6: Disc Pressure During Second Lateral Bending 59

1. INTRODUCTION

1.1 Problem Statement

The total costs of treating lower back pain in the United States exceed 100 billion dollars per year [1]. However, many patients are still left unsatisfied after spinal surgeries. A possible reason for continued pain after surgery is the effects associated with transected ligaments. The ligaments are attached between the spinal vertebrae and passively guide and stabilize the spinal movement during flexion, extension, and axial rotation [2]. One or more of the ligaments may be removed or damaged during spinal surgeries, which will likely result in the remaining elements experiencing increased loading.

The nonlinear, viscoelastic, and anisotropic behavior of ligaments make it difficult to predict how ligaments will affect the overall mechanics of the lumbar spine. Cadaver spine testing is able to determine mechanics, however, it is expensive and the testing is limited. Finite element analysis allows for repeated testing and was chosen as the method for this research.

The objective of this research is to create and validate a finite element model of the lumbar spine and test it to determine the changes that occur when a ligament is removed. This research is not limited to specific effects of certain surgeries, but will generally produce the changes that occur in the lumbar spine for each isolated transected ligament.

1.2 Summary

Chapter 2 includes a review of the literature focused on spinal anatomy and the purpose of this research. It also contains a description of spinal ligaments, their role in the biomechanics of the lumbar spine, and damage that may occur to the ligaments during surgery.

Chapter 3 includes a review of the finite element methods that have been used in modeling the spine. This chapter also includes the methods that were used to create the model used in this research.

Chapter 4 presents the bulk of the work of the thesis, and has been submitted for publication as a full-length journal manuscript. The methods section includes more details of the model generation that were not presented in Chapter 3. The results and discussion focus on the hypothesis that ligament transection increases ligament stress, potentially increases bone density, and has little effect on adjacent levels or disc degeneration.

Chapter 5 includes results and discussions that were not mentioned in Chapter 4 due to length constraints on the journal publication. These results include range of motion, vertebral body stress and load sharing.

Chapter 6 summarizes the thesis and presents possibilities for future work.

2. LIGAMENT BACKGROUND

2.1. Lower Back Pain

Lower back pain (LBP) is a major problem with an ever increasing number of patients. In the United States, more than 100 billion dollars per year is lost as a result of lower back pain [1]. There are many treatments that are used to reduce the pain caused by LBP. Initial treatments are usually non-invasive, such as strengthening the muscles surrounding the spine, but chronic cases of lower back pain are often treated with surgery.

A major cause of LBP is degenerated disc disease (DDD). DDD may lead to a decrease in disc height, disc herniation, spondylolisthesis, or spinal stenosis, each of which results in LBP. In addition, when intervertebral discs become degenerated, the compressive loads are shared by other spinal structures, including spinal ligaments.

The aetiology and treatment of LBP need to be further examined due to the complexity of the spine. Treatments that involve iatrogenic damage to or complete transection of spinal ligaments may increase the effects of LBP. Other treatments or disorders that involve increased loading in the ligaments may also result in negative long term effects.

2.2. Lumbar Spine Anatomy

The human spine is responsible for protecting the spinal cord and providing structural support, flexibility and motion. The spine is constructed of 33 separate bone structures called vertebrae. Nine of the vertebrae are fused and located in the sacrum and coccyx, while the other

24 vertebrae are articulating and separated into the cervical, thoracic, and lumbar regions. The lumbar region is located inferior to the other regions and is responsible for most of the load bearing. The lumbar region consists of the five largest articulating vertebrae and is the location of LBP. The articulating vertebrae are separated by intervertebral discs and surrounded by ligaments and muscles.

The vertebral bodies are usually numbered for ease of reference. They are separated by region and then numbered from superior to inferior. The numbering that is used in this thesis is shown in Figure 2-1. The vertebrae L1-L5 represent the lumbar region. T12 represents the most inferior vertebra of the thoracic region and is used in this research. The sacrum below the L5 will be referred to as S1 in this thesis.

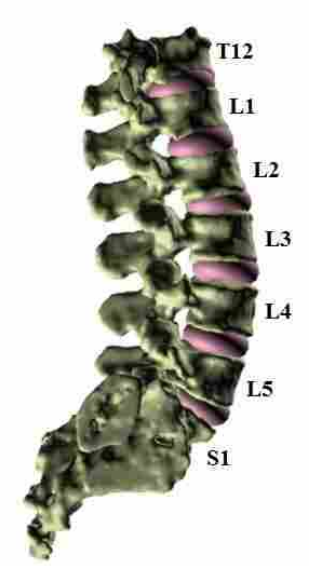

Figure 2-1: Vertebral Body Numbering

Each lumbar vertebra contains a vertebral body, pedicles, laminae and processes (Figure 2-2). The vertebral body connects to the intervertebral discs on both the superior and inferior sides. The body is responsible for carrying most of the load. Two pedicles extend from the posterior side of the body and connect to the laminae. The pedicles and laminae protect the

spinal cord as well as support the processes. The processes extend from the laminae and guide and restrict the motion of the spine.

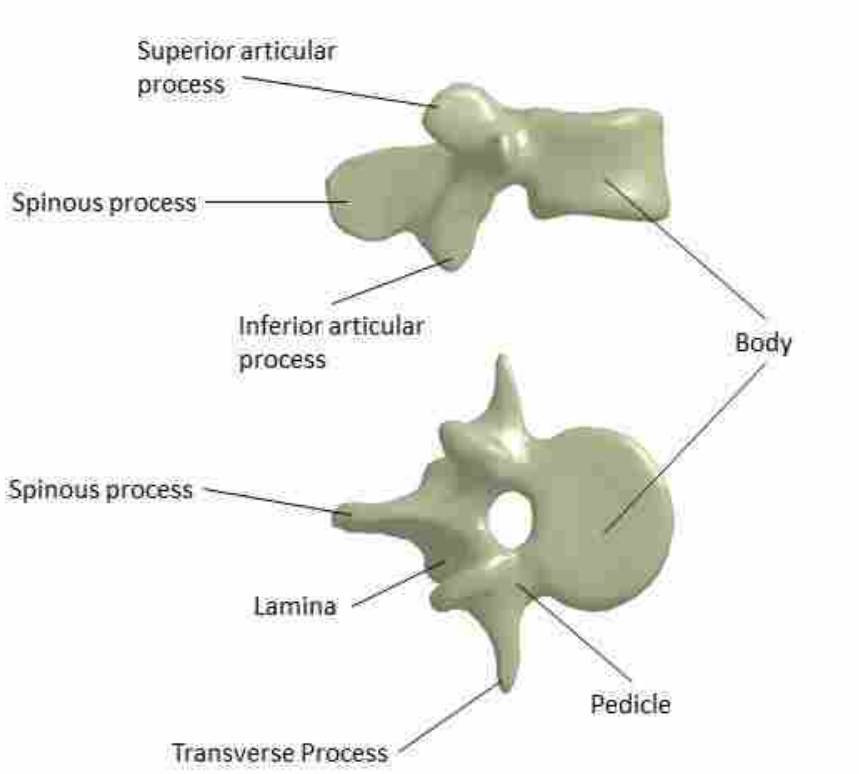

Figure 2-2: Vertebra

The intervertebral discs are attached between the vertebral bodies. The discs are constructed of an annulus fibrosus located around the nucleus pulposus. The annulus fibrosus is composed of several layers of strong fibrous tissue. The nucleus pulposus is a soft jelly-like substance. The disc absorbs energy during spinal compression, carries load, and keeps the vertebral bodies separated.

Ligaments are attached between the vertebrae and discs. They passively guide and stabilize spinal motion during flexion, extension, lateral bending, and axial rotation. Ligaments are the focus of this research and an in-depth background on ligaments is included.

2.2.1 Locations of Ligaments

There are six major ligaments that connect the lumbar vertebral bodies. They are the anterior longitudinal ligament (ALL), the posterior longitudinal ligament (PLL), the ligamentum flavum (LF), the supraspinous ligament (SSL), the interspinous ligament (ISL), and the facet joint capsules (CL). These ligaments can be seen in Figure 2-3 and are described below.

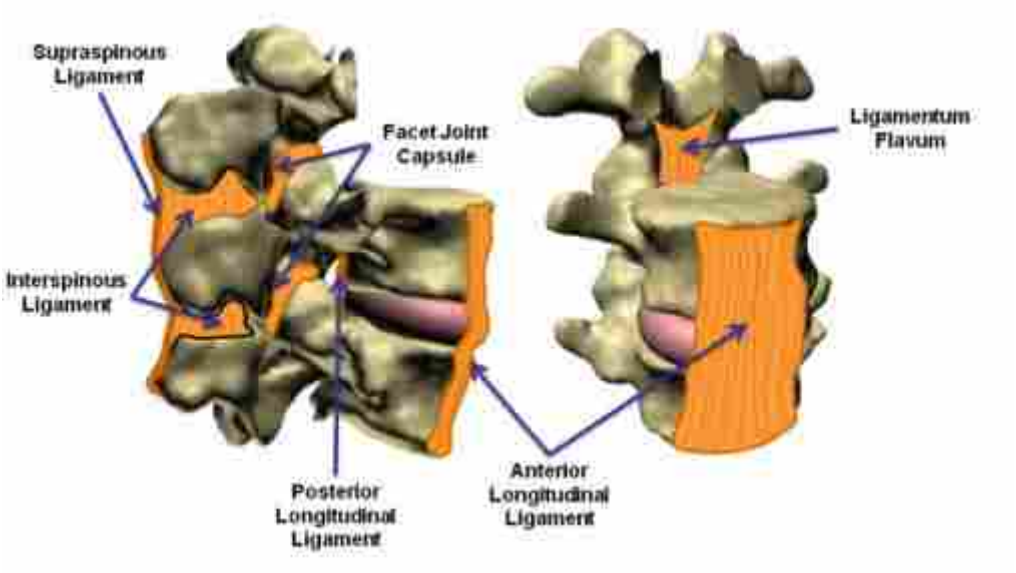

Figure 2-3: Location of Ligaments

Anterior Longitudinal Ligament – The ALL is about one-inch wide and runs along the anterior side of the vertebral bodies and intervertebral discs. It spans the spine from the base of the skull to the sacrum. The ALL is important to the resistance of extension and lateral bending.

Posterior Longitudinal Ligament – The PLL is similar to the ALL but runs along the posterior side of the vertebral bodies and intervertebral discs. It is also about one-inch wide but usually not as wide as the ALL. It runs from the base of the skull to the sacrum and forms the

front wall of the spinal canal. The PLL resists flexion and lateral bending, and plays a minor role in the resistance of axial rotation.

Ligamentum Flavum – The LF is the thickest of the spinal ligaments. It runs along the posterior wall of the spinal canal. It runs from the base of the skull to the pelvis. It fuses with the facet joint capsules and the interspinous ligament. The LF also resists flexion and lateral bending, while playing a minor role in the resistance of axial rotation.

Supraspinous Ligament – The SSL connects the posterior tips of the spinous processes. The SSL plays a major role in the resistance of flexion, and minor roles in lateral bending and axial rotation.

Interspinous Ligament – The ISL runs parallel with the spinous processes and connects consecutive vertebrae together between the spinous processes. The ISL is similar to the SSL in resistance to motion.

Facet Joint Capsules – The facet joint capsules wrap around the facet joints between the articular processes. The CL is strained in all loading directions.

2.2.2 Ligament Material Properties

Ligaments are soft fibrous tissues that are made of elastin and collagen fibers and attach one bone to another across a joint. Ligaments also guide joint movement and maintain joint congruency. Due to the structure of the ligaments, they are anisotropic. Elastic properties are much higher along the direction of the collagen fibers. Also due to the fibers, the ligaments are highly resistant to tension but not to compression.

The stress-strain relationship of ligaments being pulled in tension is non-linear. Figure 2-4 shows a representation of a typical stress-strain relationship found in ligaments.

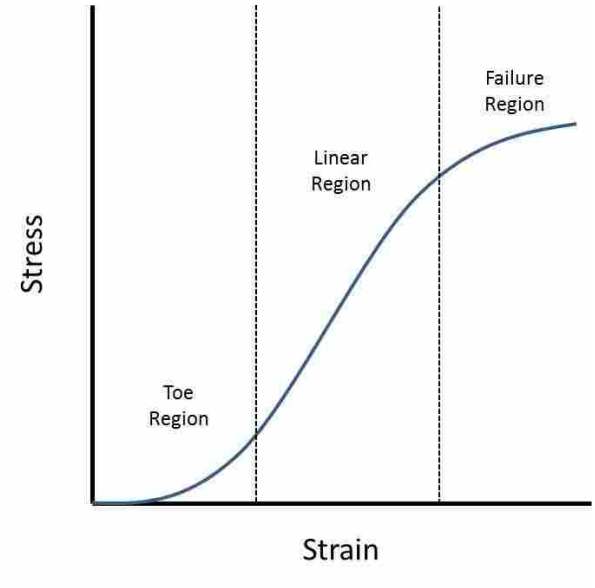

Figure 2-4: Ligament Stress-Strain Curve

For the first strain of 2-3%, the ligament undergoes a stress-strain relationship that is concave up. This first region is commonly referred to as the "toe" region. After this initial relationship, the ligament will enter a generally linear relationship and stays linear until it enters the final failure region. At this point the curve levels off [3].

Ligament behavior is also dependent on time and history due to its viscoelastic properties [4]. Therefore, the loading and unloading of ligaments do not follow the same path. Hysteresis can be seen when comparing loading and unloading. The stress-strain behavior can also be influenced by temperature, strain rate and hydration.

Many methods have been used to model ligament mechanics [3]. A more in-depth explanation of modeling ligament mechanics will be shown in Chapter 3.

2.3. Spine Surgery

Many lumbar spinal surgeries induce iatrogenic ligament damage and sometimes complete transection of spinal ligaments. A few of them are mentioned below.

Total Disc Replacement - Total disc replacement (TDR) is an invasive spinal surgery where the intervertebral disc is removed and replaced with an artificial device that connects to two vertebral bodies. TDR attempts to duplicate the natural motion of the spine, or in some cases restore the motion that had been lost in some patients. Most artificial devices have two endplates that attach to the bone of the vertebral bodies superior and inferior to the removed disc. Between the endplates is a varying form of a motion reproduction mechanism that allows for the movement. Two currently FDA approved devices include the Charite by DePuy and the ProDisc by Synthes. Many other designs are seeking FDA approval.

During surgery for TDR, the ALL or PLL may be removed or damaged. The damage to the ligaments relates to how the device is implanted. When implanted from the front, the ALL is usually removed [5]. The PLL may also become damaged or removed during surgery [6]. Current designs are looking at the possibility of implanting the device from the side in order to limit the damage caused to the ligaments. There is also concern that the height of the artificial device will limit the function of the ligaments even if they remain intact.

TDR is still a new treatment and it is still unclear as to how effective the surgery is. Some studies show that in short term cases the results have been successful when compared to fusion [7]. However, due to the recent development of these devices, there are no studies that prove that there are no long-term effects of TDR.

Interlaminar Spacer - The interlaminar spacer is another spinal surgery that relieves pain by separating vertebrae to relieve stress on the spinal nerve. The spacer is implanted by

spreading the spinous processes apart, inserting the device through the interspinous ligament, and then setting the spinous processes on the device which restricts the vertebrae from returning to their prior position. During the procedure, the interspinous ligament is damaged and might affect the biomechanics of the spine if the spacer has to be removed. Studies have shown that interlaminar spacers may reduce LBP, but there is still a debate on how effective the procedure is [8, 9].

Endoscopic interlaminar discectomy – This procedure is generally used on patients with herniated discs. A herniated disc occurs when the nucleus pulposus bulges through on opening of the annulus fibrosus. During an endoscopic interlaminar discectomy procedure, the herniated disc material is removed which relieves the pain caused by the material pressing against the nerve root. Since the ligamentum flavum sits in front of the disc for the surgeon, the ligamentum flavum must either be split or removed in order to get to the intervertebral disc and remove the material [10].

3. FINITE ELEMENT ANALYSIS BACKGROUND

A finite element model was used in this research to predict the biomechanical behavior of the human lumbar spine. After a brief introduction to finite element analysis, a review of published research on finite element spine models is included in 3.2. The remaining sections will demonstrate the methods used to create finite element models of the spine. In each of those sections, the modeling techniques that are commonly used in the research mentioned in 3.2 are listed under the *Literature* subheading. Following the literature review and under the *Current Model* subheading in each section, the methods that were used in the creation of the model used for this research are presented. Additional insights to the methods used in this research can be found in section 4.2.

3.1. Introduction to Finite Element Analysis

The main function of finite element analysis (FEA) is to simplify a complex problem into many discrete elements. Recent advances in processing capabilities of computers have made the development of complex finite element models a possibility. Complex problems can now be simplified to thousands or even millions of elements as computers are used to do the calculations.

Finite element models are low cost and easily repeatable. It is also easy to make small variations in the simulated testing conditions such as material properties or applied loads. These

benefits have led to the adoption of FEA as a standard tool for biomechanical analysis of the human spine.

3.2. Current Efforts to Model the Spine

Various finite element models of the spine have recently been published. Not all of the models that are detailed below model the lumbar spine, but all have influenced the creation of lumbar spine models and therefore details of the models are included.

Goel et al. have created a thoracolumbar model of the spine [11] as well as other models of different regions of the spine such as the cervical spine [12]. These models have recently been used to predict motion after fusion [13] and predict wear and the effect of artificial discs [14, 15].

Sharazi-Adl et al. have developed finite element models of the lumbar spine which includes one of the few models that incorporate muscles. The models have been used to predict stress during axial rotation, lateral bending, and compression [16-18], as well as finding optimal posture [19].

Ng, Teo, et al. created a model for the lower cervical spine. These models were used to predict the effects of laminectomy and facetectomy [20], the influence of preload magnitudes and orientation angles [21], and the influence of material variation [22].

Zander et al. have developed a L1-L5 lumbar model. This model has recently been used to predict the effects of pedicle-screw-based motion preservations systems [23], vertebroplasty [24], follower loads [25], and axial rotations [26]. A similar L3-L5 model was also developed [27].

Polikeit et al. created a L2-L3 model. This model has been used for predicting the effects of cement augmentation [28], and intervertebral cages [29].

Wilke et al. developed a detailed L4-L5 model [30]. This model has been used to predict the risk of disc prolapses [31], the interaction between finite helical axes and facet joint forces [32], and intervertebral disc swelling [33]. Wilke and colleagues have also recently developed a L1-L5 model based on techniques from their L3-L4 model [34].

Bowden et al. developed a validated lumbar spine model. Ligaments and disc formulation were varied in this model to better predict quality of motion [35]. Additionally, the model was used to study intervertebral disc collapse, as well as various spinal surgeries including vertebroplasty, kyphoplasty, dynamic stabilization, total disc replacement, and total facet replacement.

Rundell et al. developed a L3-L4 model used for analyzing medical devices. The model was used to predict the effects of total disc replacement positioning [36] as well as range of moduli for the nucleus pulposus [37].

Puttlitz et al. have recently developed a C3-C7 lower cervical spine model [38] as well as a L1-L5 lumbar model [39]. The L1-L5 model was validated against range of motion, intradiscal pressure, facet force transmission, anterolateral cortical bone strain and anterior longitudinal ligament deformation predictions.

3.3. Structures

The following four sections divide the model into its basic structures and present the methods of formulation for each.

3.3.1 Vertebrae

Literature

A common approach used in creating geometry for the vertebrae is computed tomography (CT) [11, 17, 28, 30]. In this approach a human cadaver spine is imaged and the geometry of the vertebral surfaces are extracted using manual or semi-automatic image segmentation schemes. Other methods used for geometry generation are direct digitation of dried or embalmed cadaveric bones [22] and manually creating or purchasing geometry based on average dimensions reported in the literature [40-43].

Different material properties are generally assigned to the cancellous bone and the outer cortical shell. Simplified, disc-centric analyses sometimes treats vertebral bodies as rigid bodies [17]. Another common method is to assume homogenous isotropic elastic properties for both cortical and cancellous bone but with different moduli [44]. A few researchers have added additional fidelity to the vertebral bodies by recognizing the relationship between CT Hounsfield number and bone mineral density. Bone mineral density has been strongly linked with cancellous bone stiffness and strength. Thus, if the CT data is calibrated using a bone mineral density phantom, the CT data can be related to bone mineral densities [35, 36, 39]. This process is known as quantitative computed tomography (QCT) [45]. To achieve even higher architectural resolution of the cancellous bone trabecular structures, micro-CT scanners can also be used to determine trabecular structure and assign material properties on a micro-level. These models are highly fidelic to the bone architecture, but because of their necessarily high mesh density, they have (so-far) been limited to linear elastic, non-contact models of small regions of interest.

Current Model

The geometry used in this research was based on QCT images of a 65-year-old female cadaveric spine. Surfaces for the vertebral bodies were extracted semi-automatically using Analyze (Mayo Clinic, Rochester, MN). Material properties for the cancellous bone were assigned using correlated bone mineral densities. The correlation was made by comparing densities of the spine to a calibration phantom that was imaged with the spine. For every element, an anisotropic elastic modulus in each direction was assigned using equations found in the literature [45, 46]. The equations can be found in more detail in section 4.2.1.

An example of the vertebra material code can be found in C.2.2. This code defines the nonlinear relationship between material properties to Hounsfield numbers extracted from the CT data. Hounsfield numbers are extracted based on the physical location of each node within the three-dimensional CT data set. Each node in the model is assigned anisotropic elastic moduli based on the relationship between Hounsfield number and material properties. The element properties are then determined based on averaged values from the attached nodes. Consistent with previously work, a 0.4 mm thick cortical shell was then added around the cancellous bone and assumed to be homogenous isotropic elastic with an elastic modulus of 12GPa.

The vertebral bodies where the loading conditions occurred were assigned to be rigid bodies. These include the S1 (where the model was fixed) and the T12 (where the load was applied). An example of the material code can be found in C.2.1.

3.3.2 Disc

Literature

The nucleus pulposus is commonly modeled as an incompressible fluid [20, 44]. Recent studies have commonly used rubber-like hyperelastic properties instead. The Neo–Hookean and Mooney-Rivlin models are common in this approach [30, 35]. When modeling the annulus fibrosus, researchers can either take an isotropic approach where the ground substance and the cross fibers are modeled individually [28, 30], or a continuum anisotropic approach [20, 44]. More complex constitutive models have also been used [39].

Current Model

The model used in this research took the continuum approach when modeling the annulus fibrosus. The geometry was created in Pro/Engineer (PTC, Needham, MA). The upper and lower disc geometry was taken from the vertebral body geometry. The surfaces were then created in Pro/E by connecting the upper and lower geometry. The nucleus pulposus was created to be around 40% - 50% of the volume of the disc at each motion segment level. The annulus fibrosus was split equally based on diameter into inner and outer sections. An example of the disc geometry connected to a vertebral body can be seen in Figure 3-1. The red inner region corresponds to the nucleus pulposus, while the blue and green regions correspond to the inner and outer annulus fibrosus regions, respectively.

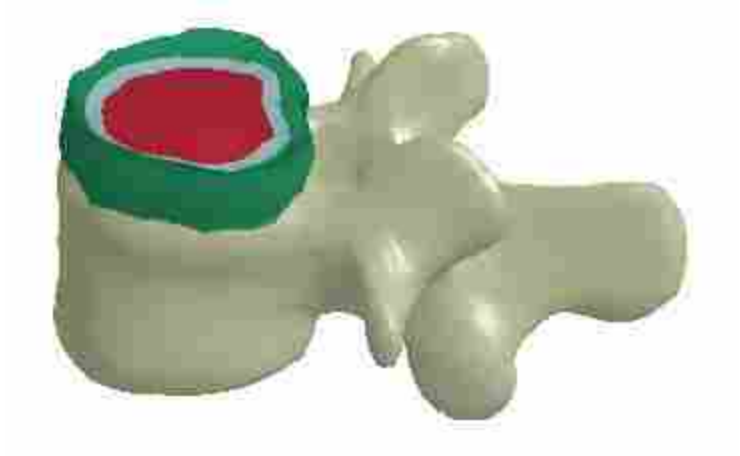

Figure 3-1: Intervertebral Disc Geometry

Both the inner and outer sections were modeled using anisotropic elastic elements with different properties for each. The nucleus pulposus was modeled using a Mooney-Rivlin formulation. Details of the materials can be found in 4.2.1 and the material code for an intervertebral disc can be found in C.2.3.

3.3.3 Muscles

Literature

Muscles are important to the active stabilization of the human spine (e.g., resistance to viscoelastic drift of spinal posture due to the soft tissues of the spine). Muscles are difficult to model due to significant differences between subjects, and their action is highly activity-dependent. Several researchers have estimated muscle forces during various activities and have applied them to their models [19, 47, 48] and other studies have considered the importance of adding muscles [15]. Muscles are sometimes simulated in a finite element model by adding forces with determined magnitudes, directions and locations.

A common approach used in many models to simulate upper body weight and muscle forces is the addition of a follower load [49]. The follower load compresses the spine through a path parallel to the spinal cord that runs through the middle of the vertebral bodies and nucleus pulposus. The load simulates the compression and stabilization caused by upper body weight and stabilizing muscle forces.

Current Model

The model used in this research uses the follower load concept to duplicate the stabilizing forces of the muscles in compressing the spine. A discrete beam was created through the center of the vertebral bodies and the nucleus pulposus. An initial force of 444N was added to create the compression. The material code for the follower load can be seen in C.2.5.

3.3.4 Ligaments

Literature

Various levels of complexity with both material properties and geometry have been used to model spinal ligaments. The least complex, and most common method that is commonly used is simplifying the ligaments to be two-node tension-only cable elements with linear elastic spring properties [12, 17, 20, 28, 30, 39, 50]. This method is attractively simple, however it fails to capture shear forces, material anisotropy and the complex interactions of synergistic ligament interactions. Shell elements overcome these limitations, while preserving many of the computational advantages of the cable element approach [35]. Volumetric representations of ligament geometry are uncommon, due to the high aspect ratios or very high discretization levels required by these long, thin sheets of soft tissue material. However, at least one researcher has

developed a volumetric ligament representation based on magnetic resonance imagining (MRI) [32]. Due to the nonlinear nature of the ligaments, researchers have defined material properties with force-displacement [39] or stress strain curves [35].

Current Model

In the model used in this research, ligaments were constructed with elements known in LS-Dyna as "fabric" shell elements [51]. These elements support complex loading in tension and shear, but not compression. Geometry was constructed by attaching an area of sheet elements to the anatomically correct locations of the vertebrae. Elements were assigned stress-strain properties based on the literature [35, 52]. Details of the ligament formulation can be found in 4.2.1. An example of the material code for one ligament can be found in C.2.4.

3.4. Mesh

Literature

Hexahedral elements are commonly used to model the vertebral bodies and intervertebral discs [11, 20, 28, 30, 39, 47]. Models using tetrahedral elements are easy and quick to construct due to automatic tetrahedral meshing software [36] , but they are used less frequently. Common verification techniques usually involve doubling the amount of elements in the model to see if the changes in maximum stress are significant. Beam or shell elements are also commonly used in the formulation of ligaments. However, volumetric elements have been used in ligaments as well [32].

Current Model

The model used in this research consisted of 234,011 elements. Elements were created using a commercial finite element preprocessor (TrueGrid, XYZ Scientific Applications, Inc., Livermore, CA). Hexahedral meshing for all of the elements besides the vertebrae was straightforward. A tetrahedral mesh of the model was also created to compare accuracy, but the tetrahedral model was unable to achieve stress convergence even when of 1,000,000 elements were used. Therefore, the hexahedral mesh was used instead of the tetrahedral mesh. In order to mesh the vertebrae, a vertebra was separated into the 6 different parts seen in Figure 3-2. Advanced meshing techniques were used to create the 6 meshes separately before connecting them together.

Figure 3-2: Parts for Vertebrae Meshing

A second model consisting of 465,082 elements was created and used to successfully verify the model's discretization level (stress convergence) during compression and flexion. Figure 3-3 shows both of the models that were used for stress convergence. Stress convergence

was ensured by running both models in compression and flexion and verifying that deviations in stress contours were minimal and that variation in maximum stress values were less than 5%. Figure 3-4 shows the quality of the elements based on a histogram of Jacobians. The Jacobians ranged from .0001 to 6.97. However, there were only 19 elements below .01 and about 100 over 4. Most of the worst elements were located on the transverse processes.

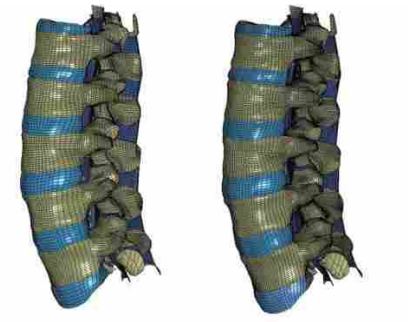

Figure 3-3: Mesh and Double Mesh for Stress Convergence

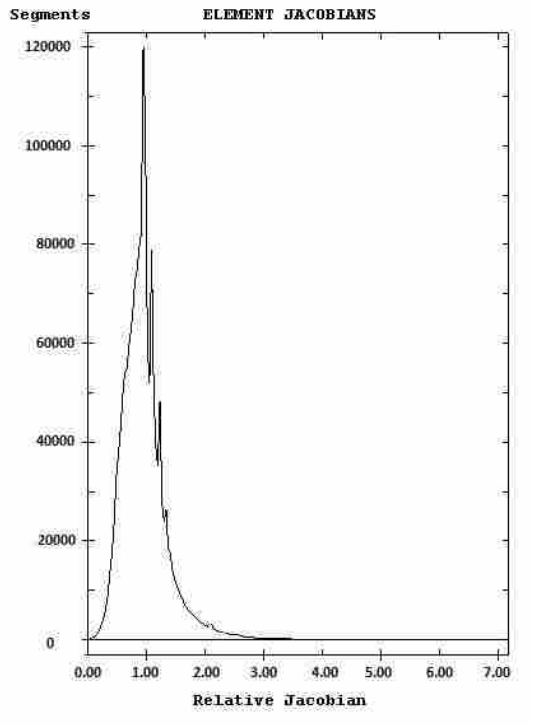

Figure 3-4: Element Jacobians

3.5. Contact

Literature

Models must predict the contact that occurs between adjacent articular processes. This may be addressed in finite element solvers by using so-called "contact" elements, by using a penalty approach algorithm based on the modulus of the mating surfaces, or by enforcing contact using an iterative augmented Lagrangian approach. Implementation of these methods varies by solution technique and finite element implementation.

Current Model

The solver used in this research was LS-Dyna (LSTC, Livermore, CA). Contact was implemented using a surface-to-surface penalty algorithm. The contact options (in LS-DYNA keyword format) for each of the contacting surfaces can be found in C.1.

3.6. Loading

Current Model

The model was tested in the 6 primary loading directions (flexion, extension, left and right lateral bending, left and right axial rotation). The directions are shown in Figure 3.4. During loading the S1 was fixed and a pure moment was added to the T12. 6 Nm was applied for each direction except for flexion in which 8 Nm was applied. The follower load was applied before the loading moments to allow the compression to stabilize before further loading. Because this initial compression was the same for each case, the compression output was saved and all of the load cases began from that point using a dynamic restart technique. Loading code

for the initial compression (LS-DYNA keyword format) as well as an example of the code added for a particular loading case can be found in C.1. Supercomputer commands for the compression loading as well an example of a restart for the different loading cases can be found in C.3.

Because an explicit (rather than an implicit) nonlinear solution technique was utilized, damping was needed to stabilize the analysis. A damping coefficient of 2 Ns/mm was used for stability of the compression, and then changed to 0.19 Ns/mm for the loading cases. The damping coefficient for the loading cases was determined from kinetic energy frequencies of a model run without damping.

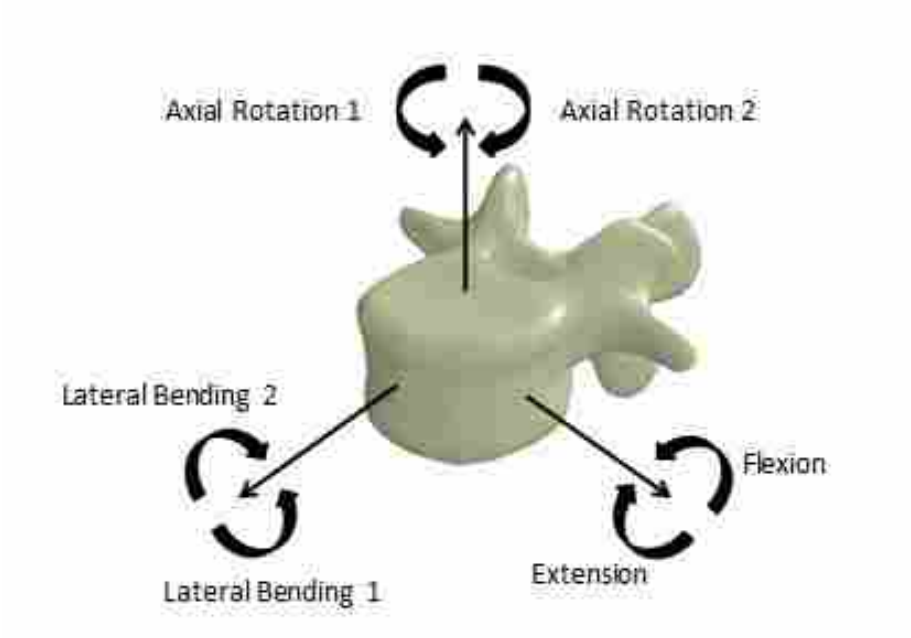

Figure 3-5: Loading Directions

3.7. Validation

Literature

In order to predict future behavior of the spine, a finite element model must match experimentally observed behavior. A majority of the models mentioned in this review, either

have no mention of validation, or have very simple methods of validation. Two of the more common methods of validation include comparing range of motion and disc pressure results to the results obtained from experimental testing. Although this may be sufficient for some models, it is also important to validate the model against the same data that will be measured. For example, if the research requires range of motion data, the model must be validated against range of motion. However, if the research also requires cortical strains, a range of motion validation is not sufficient. Likewise, for analysis that will investigate and report interverbral disc pressures, the model should also be validated against intervertebral disc pressure.

Current Model

The stress converged model was validated by comparing data predicted by the model to experimental data presented in the literature. The following parameters were used for comparison:

Range of motion – Loading moments were applied to the T12 while fixing the S1 in flexion/extension, lateral bending and axial rotation. Kinematic data of the model were compared against reported experimental studies [53] and data from testing done on the spine used for the geometry.

Quality of motion – To ensure an even more accurate prediction of spinal kinematics, the applied moment was plotted against the angular displacement to verify that the data followed a physiological nonlinear path as presented in the literature [35, 54]. Figure 3-6 shows range and quality of motion results for the T12-L1 functional spinal unit.

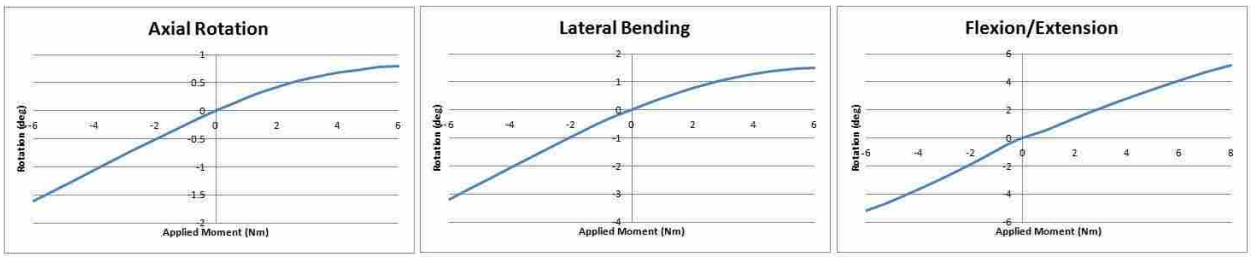

Figure 3-6: Motion Validation

Disc Pressure – After the model was compressed, disc pressure data was collected by averaging the pressure of a small spherical region of elements located in the center of the nucleus pulposus. This average simulates the experimental data collected by probes. The disc pressures were compared to data presented in the literature [55]. The literature data is shown in Figure 3-7 and selected disc pressures from compression results in the model used in this work is shown in Figure 3-8.

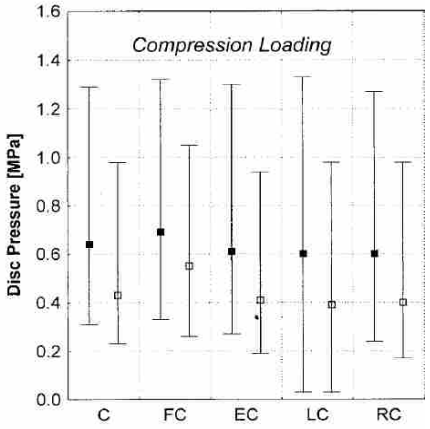

Figure 3-7: Disc Pressure Data Frei et al. (2001), Spine.

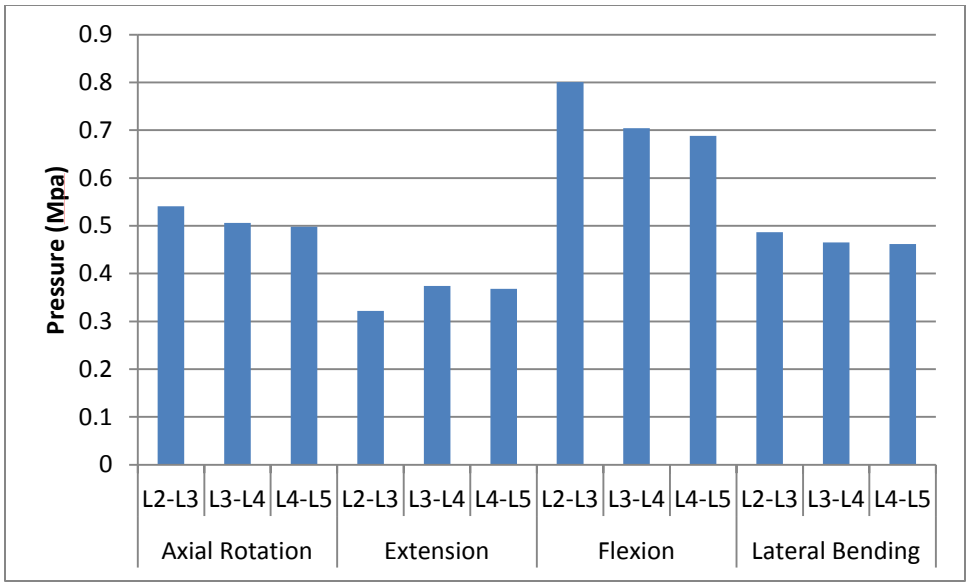

Figure 3-8: Disc Pressure During Compression

Cortical Strains – Cortical strain comparisons were made by comparing the maximum principal strains from the model to the experimental data in seven different locations of the vertebral bodies [55]. Table 3-1 compares the limits of the range recorded in the literature as well as the calculated strain for the model used in this thesis.

Table 3-1: Cortical Maximum Principal Strains (Microstrain)

Location	Lower Limit	Upper Limit	Calculated
Anterior Endplate	177	3168	431
Posterior Endplate	464	2032	803
Left Endplate	137	4497	474
Right Endplate	273	2548	387
Right Rim	215	463	298
Anterior Rim	431	916	670
Left Rim	192	711	341

Instantaneous Axes of Rotation – The axes of rotation for each of the functional spinal units during flexion/extension were calculated and compared to locations found in the literature as shown in Figure 3-9 and 3-10 [56].

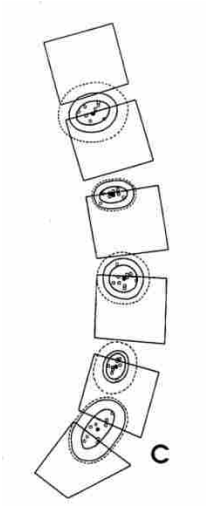

Figure 3-9: Location of Axes of Rotation Pearcy and Bogduk, (1998), Spine.

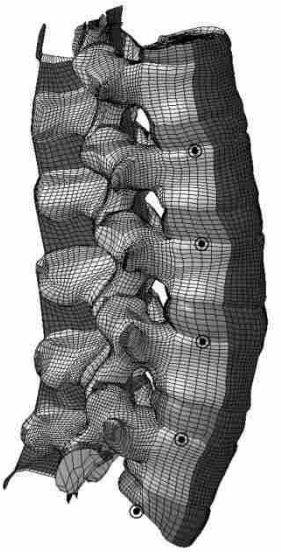

Figure 3-10: Location of Axes of Rotation in Current Model

4. IMPLICATIONS OF SPINAL LIGAMENT TRANSECTION

4.1. Introduction

Lumbar spinal ligaments form a coordinated network of passive attachments between adjacent vertebral bodies that guide and stabilize spinal movement [57, 58]. Previously published work has identified the synergy in mechanical roles between lumbar spinal ligaments [2, 58]. This synergy dictates the load transfer within the spinal ligament network consequential to damage. Cadaveric spine testing work has also elucidated the response of the spine to sequential transection of spinal ligaments, virtually always by first cutting external ligaments then progressing to deeper ligaments [59-61]. Zander [62], reported on the changes in segmental rotation and ligament load sharing as a consequence of isolated ligament transections using a finite element model. Similarly, Gudavalli [63] used a finite element model to examine load sharing and ligament strain in flexion as a result of ligament transection. However, the biomechanical consequences of isolated ligament transection on ligament stress transfer, bone remodeling, and intervertebral disc pressure have not yet been reported. This topic has a clear clinical relevance, due to the prevalence of iatrogenic (surgeon-induced) ligament damage during common spinal surgeries.

Many lumbar spinal surgeries induce iatrogenic ligament damage and sometimes complete transection of spinal ligaments. For example, most current total disc replacements (TDR) are implanted using an anterior approach that requires removal of the anterior

longitudinal ligament [64], and resection or excess stretching of the posterior longitudinal ligament [6]. Anterior interbody fusion damages or transects the anterior longitudinal ligament, while posterior interbody fusion similarly damages or transects the posterior longitudinal ligament, with potential injury to the ligamentum flavum, interspinous ligament, and superspinous ligament [65, 66]. During endoscopic interlaminar discectomy, the ligamentum flavum is typically removed or split [10. Interlaminar spacers require transection of the interspinous ligament {Lo, 2010 #10], with possible damage to the supraspinous ligament. Microdiscectomy either damages or transects the ligamentum flavum and can induce damage to any of the posterior ligaments [67].

In the present work, isolated iatrogenic ligament transection was investigated using a nonlinear finite element model of the lumbar spine. Finite element models of the lumbar spine have become a standard tool for predicting both the normal and pathological mechanics of the lumbar spine [11, 17, 20, 28, 30, 35, 39, 47, 68, 69]. They provide opportunities for repeated testing of the same spinal segment under distinct clinical conditions that eliminate the high subject-specific variability found in clinical testing and cadaveric testing. They also provide direct predictions of mechanical stress and strain that are very difficult to obtain through laboratory testing.

The fundamental hypothesis of the work was that isolated ligament transection would increase stress in synergistic elements of the spinal ligament network, and induce changes in vertebral bone remodeling. We also postulated that changes in intervertebral disc pressures would be minimal, and that the effects of isolated ligament transection would primarily be confined to the operative level. This hypothesis was tested through repeated analysis of a

carefully validated finite element model of the lumbar spine in the primary spinal bending modes.

4.2. Methods and Materials

4.2.1 Finite Element Model

A three-dimensional, hexahedral finite element model of the ligamentous lumbar spine (T12-S1) was created based on quantitative computed tomography (QCT) data from the donor spine of a 65 year-old female (Figure 4-1). Vertebral geometry was semi-automatically segmented from the QCT data using Analyze (Mayo Clinic, Rochester, MN). Intervertebral disc geometry was similarly extracted based on thresholded QCT values. The cortical bone on the surfaces of the vertebral bodies was created with shell elements. Spinal ligaments were modeled using nonlinear, tension-only, "fabric" shell elements [51]. Table 4-1 summarizes the material formulations and properties in the model. A sensitivity study regarding these material choices was recently published in this journal [35].

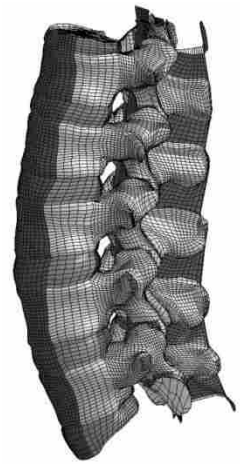

Figure 4-1: Hexahedral Finite Element Model of the Lumbar Spine

Table 4-1: Material Formulations and Properties

Structure	Formulation	Modulus	Poisson's ratio	References
Cortical bone	Isotropic, elastic shell elements	12000	0.2	[28, 70]
Cancellous bone	Density dependent anisotropic, elastic hex elements	$E_z=4730\rho^{1.56}$ (a) $E_x= 0.42E_z$ $E_y= 0.29E_z$	0.23, 0.4, 0.38 (b)	[45, 46]
Nucleus pulposus	Mooney-Rivlin hex elements	0.5, 0.05 (c)	Incompressible	[35, 71]
Inner annulus fibrosus	Anisotropic, elastic hex elements	5.6,0.34,0.19 (d)	1.86,0.88,0.14 (d)	[72]
Outer annulus fibrosus	Anisotropic, elastic hex elements	17.45,0.27,0.19 (d)	1.77,0.33,0.14 (d)	[72]

*NOTE (a) The modulus in the z direction represents the modulus in the axial (superior-inferior) direction and is calculated from the bone mineral density. The moduli ratios in the orthogonal directions were obtained from the literature. (b) Poisson's ratios for the three orthotropic directions. (c) Mooney-Rivlin constants. (d) Orthotropic moduli and ratios.

Heterogeneous cancellous bone properties were assigned to the vertebral bodies based on calibrated bone mineral densities obtained from the calibrated QCT scan data. Custom software interrogated the bone mineral density corresponding to the spatial location of each computational element. Bone mineral densities were correlated with anisotropic tissue moduli through the use of quantitative relationships previously reported by Morgan et al. (2003) and Ulrich et al. (2009). [45, 46]. This methodology is consistent with previously published work [37]. The exponential relationships were implemented as piecewise linear functions. Shell elements were added around the cancellous bone to create a homogeneous, isotropic cortical layer similar to previously published work [11, 28]. The contact between the facets of each vertebral body was characterized with a non-friction surface-to-surface penalty method.

Special care was made to ensure an accurate geometric and material characterization of the spinal ligaments. Traditional techniques for representing spinal ligaments using nonlinear spring elements [12, 17, 20, 28, 30, 39, 50] are adequate for mimicking spinal flexibility. However, spring elements are incapable of capturing the nonlinear shear coupling induced by the complex geometry of the spinal ligaments and the insertion of the ligaments into one another. For example, the interspinous ligament directly inserts into the supraspinous ligament. Because

of the thin cross-section of these ligaments, representation using solid elements (hexahedral or tetrahedral) results in high aspect ratios that can yield inaccurate results. Thus, in the present work, spinal ligaments were represented in the model using tension-only "fabric" shell elements [51]. Shell elements have the advantage of capturing the full three-dimensional deformation and stress fields in the ligaments (including shear coupling), while minimizing the computational burden imposed on the solution process.

The major spinal ligaments were represented: anterior longitudinal ligament (ALL), the posterior longitudinal ligament (PLL), the ligamentum flavum (LF), the supraspinous ligament (SSL), the interspinous ligament (ISL), and the facet joint capsules (CL). The transection of these ligaments will be represented in the present work by placing an (x) in front of the ligament abbreviation (i.e. xALL for the transection of the ALL). The intertransverse ligament (ITL), which is often represented in FE models [17, 28, 30, 36, 50, 73], was purposely neglected in the current work. Careful dissections in our laboratory have indicated that less than 10% of lumbar spine cadaveric specimens show any evidence of ligamentous tissue between the transverse processes of adjacent segments. This finding has been confirmed in the literature [74].

Ligament cross-sections were assigned to the tension-only shell elements based on reported cross-sectional areas from the literature [52]. Nonlinear material constitutive relationships were applied to each ligament based on previously reported work [52] and were implemented as piecewise linear functions as shown in Table 4-2. The properties for the CL were also taken from the literature, but simplified to be linear [75].

Table 4-2: Ligament Properties

Ligament	Cross-sectional area	Constitutive Relationship - Strain, Stress [(a)]		
		A	B	C
ALL	65.6 mm^2	0.12, 1.15	0.44, 9.11	0.57, 10.3
PLL	25.7 mm^2	0.11, 2.04	0.34, 16.19	0.44, 20.8
LF	39.0 mm^2	0.07, 2.04	0.19, 9.14	0.25, 10.38
ISL	15.1 mm^2	0.17, 0.95	0.38, 5.86	0.54, 6.69
SSL	15.1 mm^2	0.17, 0.95	0.38, 5.86	0.54, 6.69
CL	0.074 mm[(b)]		E=0.3 [(c)]	

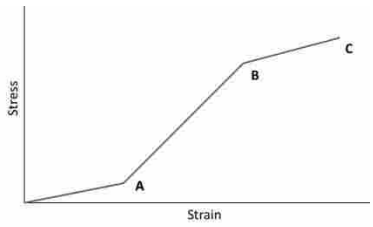

*NOTE (a) The constitutive relationships for the all of the ligaments except for the facet joint capsules were modeled using a piecewise linear representation. The modulus changes at inflection points A, B, and C, which are listed for each ligament as the stress-strain relationship. (b) The ligament size for the CL is reported as thickness. (c) The facet joint capsules were simplified as linear elastic with the stated modulus.

The intervertebral disc was modeled in three sections: the nucleus pulposus and the outer and inner annulus fibrosus. The nucleus pulposus constitutive response was modeled using a hyperelastic Mooney Rivlin material [71]. This material in the nucleus pulposus along with the ligament properties presented earlier have been shown to improve the quality of motion during spinal bending [35]. The inner and outer annulus fibrosus were modeled using transversely anisotropic elastic properties [72].

4.2.2 Verification and Validation

In order for the model to correctly predict spinal behavior, the model was stress converged to tet mesh resolution. Another model of the same geometry was created with twice as many elements in order to verify stress convergence and mesh discretization. This model contained 465,082 elements compared to the 234,011 in the model used for testing. Both models were compressed and maximum stresses were within 5%.

The stress converged model was validated by comparing data to experimental data presented in the literature. Validation of this model was discussed in section 3.7.

4.2.3 Simulated Testing Procedure

The finite element model was tested in flexion, extension and axial rotation using LS-Dyna [51]. A compressive follower load was added to simulate muscle tension and upper body weight [49]. The reference configuration of the model was evaluated with all of the ligaments intact. The model was tested by applying a moment to the T12 segment while constraining the sacrum from translation and rotation. The following six different moments were applied: 6 Nm in each (left-right) axial rotation, 6 Nm in each (left-right) lateral bending, 8 Nm in flexion, and 6 Nm in extension. Results for load sharing, disc pressure, range of motion, stress, and strain energy were recorded for comparison. The ALL between the L3 and L4 was removed from the model and the six tests were run again and data was recorded. The ALL was then replaced and the PLL between the L3 and L4 was removed from the model. The six tests were executed again, and data was recorded. The same process was repeated for the CL, LF, ISL and SSL. For each removed ligament, the six tests were executed, and data was recorded. During any given test, there was only one ligament missing from the model, and it was always removed between the L3-L4. Thus, a total of 42 separate nonlinear finite element simulations were performed. Each finite element simulation required approximately 890 cpu hours on a hex-core Intel Westmere (2.67 GHz) workstation with 24 GB of core memory. The data from each simulation were extracted and compared to the intact condition.

4.3. Results

The transection of a ligament generally caused an increase in maximum stress in the synergistic elements of the remaining ligament network. Figure 4-2 shows ligament stress results for each of the 42 simulations.

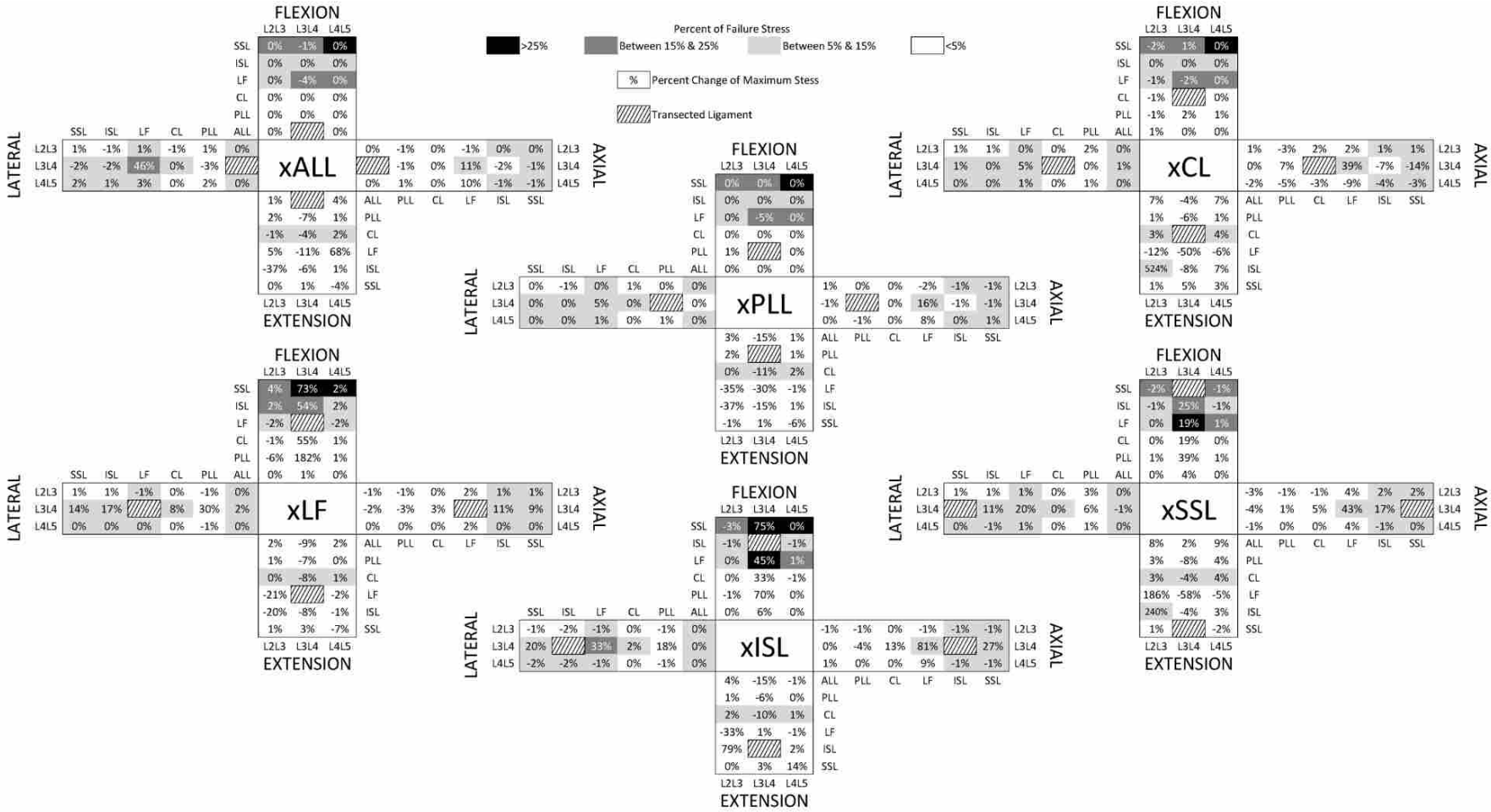

T-charts displaying changes in ligament stress due to isolated transection of each lumbar spinal ligament. Each mode of loading (flexion, extension, axial rotation, lateral bending) is indicated on a

Figure 4-2: Ligament Stress Changes

The transected ligament is indicated in the center of each "T-Chart". On the T-chart, mode of loading is indicated for each leg of the chart (left-right motions for lateral bending and axial rotation were averaged). The percent change in maximum stress in each ligament due to that transection is listed at both the transected level (L3-L4), as well as the adjacent levels (L2-L3, L4-L5). Highlighted cells show the amount of stress that each ligament undergoes as compared to the ligament's reported failure stress. Reported ligament failure stresses are given for reference in Table 4-2 (point C). Thus, large percentage changes that are shaded are of particular interest.

Substantial changes in the stress magnitude of highly stressed ligaments were observed subsequent to the transection of the LF, ISL, or SSL between the L3 and L4. The removal of one of these ligaments creates large increases in stress in the other two ligaments, especially during flexion. Figure 4-3 shows the stress contours of the ligament network due to transection of these three ligaments during flexion.

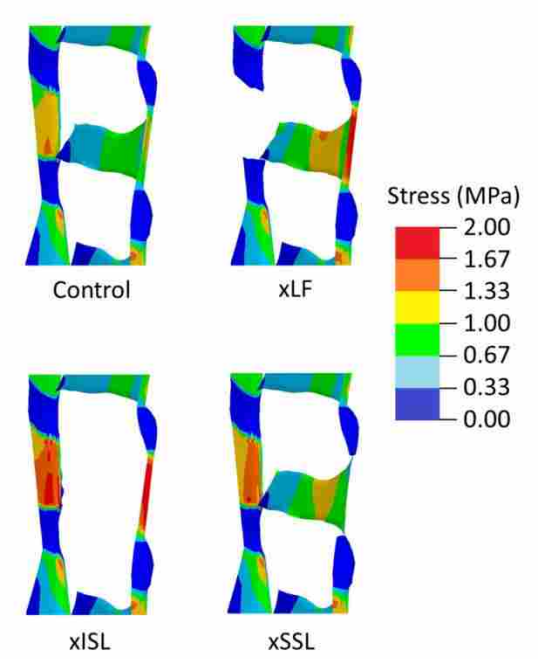

Figure 4-3: Stress Contours During Flexion

Of all the lumbar ligaments, transection of the PLL had the least impact on the stresses in the surrounding ligament network. Similarly, transection of the ALL was primarily consequential to a single ligament (the LF) during a single mode of loading (lateral bending). Virtually all of the major changes in ligament stress occurred at the index (transected) level. Notable exceptions were seen with the removal of the SSL or the CL. The removal of the CL increased stress levels in the ISL during extension at the inferior level, while the removal of the SSL increased the stress in both the LF and the ISL in extension at the inferior level.

Ligament transection resulted in no major changes in intervertebral disc pressure in the nucleus pulposus as shown in Figure 4-4. During all loading cases, the intervertebral discs generally carried between 80-82% of the load. While the distribution of the remainder of the load throughout the surrounding tissues changed, the pressure within the discs remained fairly constant. A full summary of the disc pressures in all loading cases can be found in Appendix A.

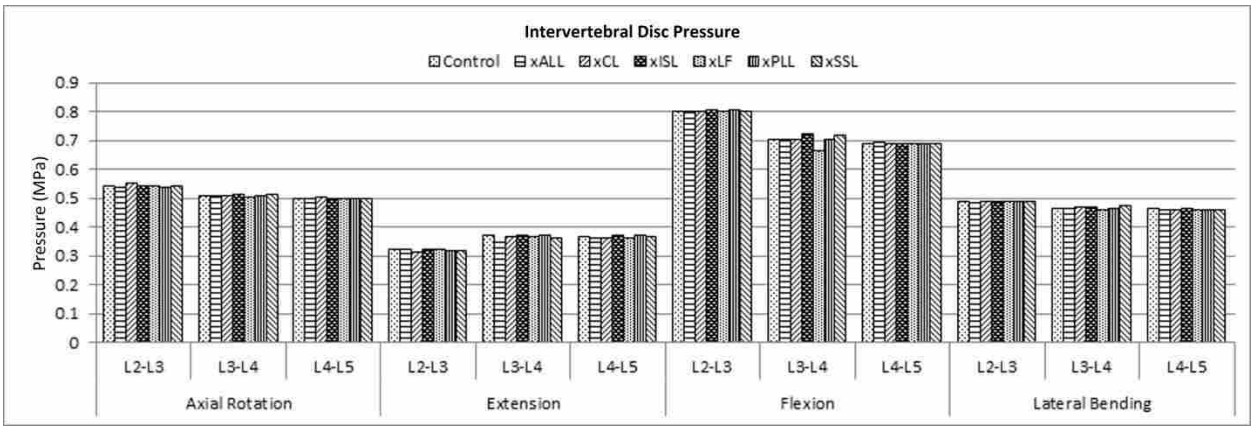

Figure 4-4: Intervertebral Disc Pressure

Strain energy was calculated in the vertebral bone for each loading case to evaluate bone remodeling potential (Huiskes et al., 1987, Fyhrie and Carter, 1986). Changes within 0-50% of the nominal strain energy from the intact case were assumed to enact little to no bone

remodeling. Changes above 50% are highlighted in Figure 4-5 for flexion, changes between 50-100% are marked as "Increase" or "Decrease", while changes above 100% are marked as "Major Increase" or "Major Decrease". With transection of the LF, ISL, or SSL, large changes in strain energy can be seen in the processes and the pedicles. Changes in vertebral strain energy during the other modes of loading were almost exclusively contained within 50% of the nominal values and were assumed to induce little to no bone remodeling.

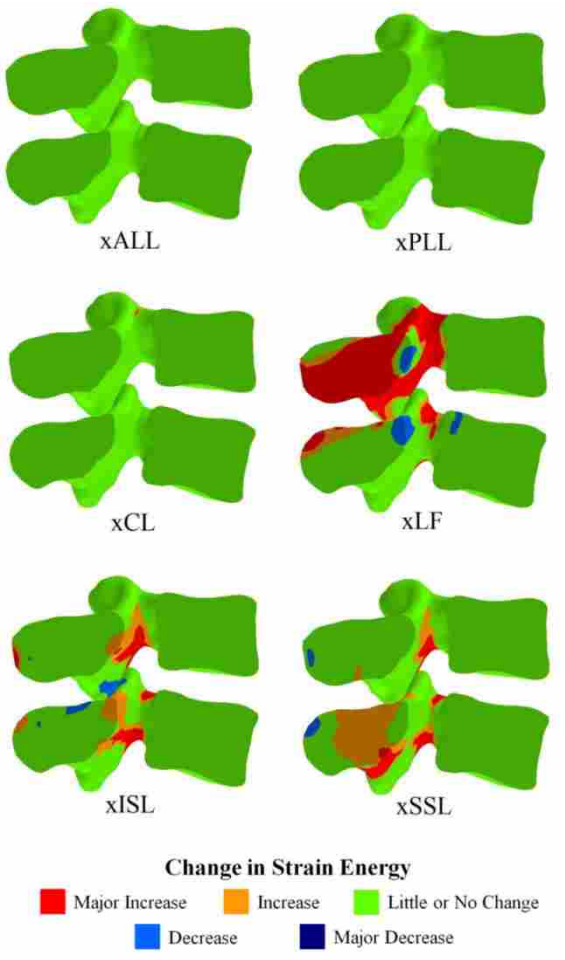

Changes in vertebral strain energy (correlated to bone remodeling) during flexion as compared to the intact simulation are reported for each transected ligament simulation at the index (transected level). The vertebrae are split through the sagittal plane to allow visualization within the bone. "Little or no change" indicates a change between -50% and 50% of the nominal (intact) value. Major changes are any increases above 100% or below -100%.

Figure 4-5: Change in Strain Energy

4.4. Discussion

Isolated ligament transection virtually always increased stresses in synergistic elements of the spinal ligament network. This finding confirmed our initial hypothesis and supports a conclusion that ligament transection may increase the potential for overload or fatigue damage in these elements. Our findings suggest that increased injury potential is greatest in the posterior ligaments (ISL, SSL, LF) at the level of the transected ligament. When any of these ligaments is transected, the remaining ligaments experience significantly higher stresses that approach their reported quasi-static failure stresses.

A full bone-remodeling simulation [76, 77] was beyond the scope of the present work. However, consistent with recently published work by other authors [37, 78, 79], we examined the changes in strain energy in the cancellous bone as a result of surgery to identify an initial bone remodeling "stimulus". We found that isolated spinal ligament transection generally induced a stimulus that would lead to increased bone density, with a few exceptions localized around the transected ligament insertion sites.

The removal or damaging of isolated spinal ligaments shows minimal changes in disc pressure and therefore seems to play no major role in disc degeneration. There was minimal variation of disc pressure in the discs during any of the loading conditions. This is likely due to the large percentage of the load the discs carry. A small increase in the load has a large of effect on the surrounding elements, but is relatively small for the discs. This minimal effect on disc pressure is likely in the disc at the transected level as well as the adjacent levels.

Finite element modeling of complex geometries and material responses, such as those found in the spine, carry a high burden of verification and validation [80]. Therefore, special care was taken to insure that the predictions made by the model were as accurate as possible.

The model was validated against experimental data for range of motion, quality of motion, cortical strains, disc pressures, and axes of rotation. Because the present work investigated ligament stresses and ligament transection, fabric shell elements were chosen for the ligaments to allow for more accurate predictions than are possible using the more traditional cable elements.

Because the model did not take into account ligament prestrain, it is likely that the stresses in the ligaments are somewhat higher than reported. This concern is common to virtually every finite element simulation of the spine. Measurement of ligament prestrain is challenging, and has not yet been reported for most spinal ligaments.

Since the model only considered one transected ligament at a time, the current results are unable to show the coupled effects of multiple damaged or transected ligaments. For example, it is possible that a surgery that requires the transection of the ISL will lead to the SSL being damaged. Evaluation of coupled ligament transection remains a topic for investigation.

Ligaments play an important role in the biomechanics of the lumbar spine. The present work shows that ligament transection may increase stresses in the remaining ligaments as well as induce bone remodeling. These impacts should be considered for any clinical procedures that may damage or require the removal of a ligament.

5. ADDITIONAL INSIGHT

5.1 Additional Results

Range of motion was computed for all of the loading conditions. The percent change for each isolated transected ligament loading case is shown in Figure 5-1. There were minimal changes in range of motion during axial rotation and lateral bending. At the transected level, there was a large increase in motion during flexion when the LF, ISL, or SSL was removed. There was also a trend of decrease in motion at the transected level for most of the transection cases.

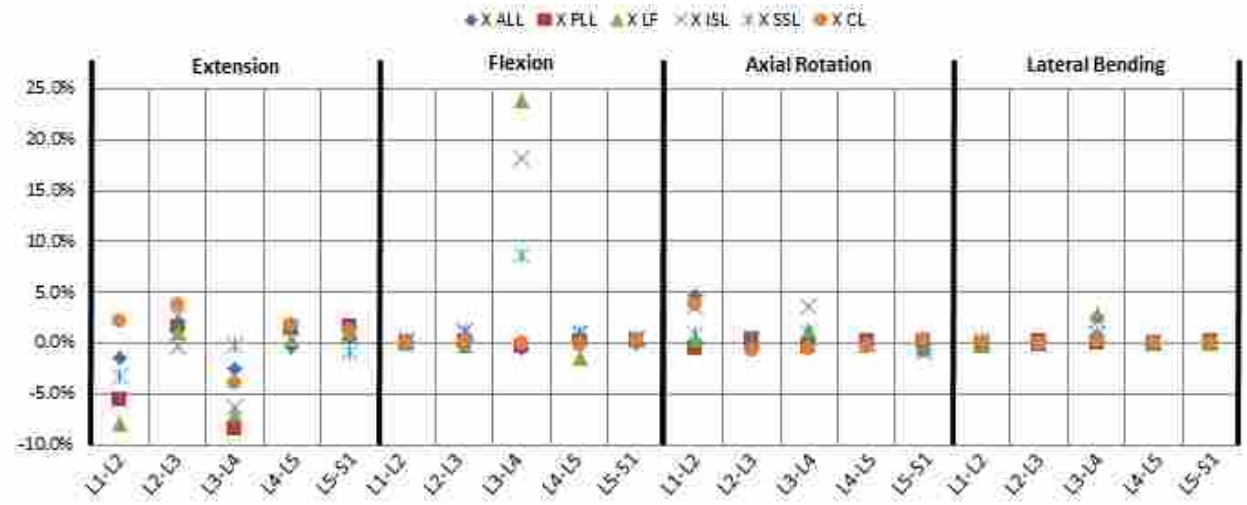

Figure 5-1: Change in Range of Motion

The maximum stress in the pedicles was also analyzed and recorded in Figures 5-2 through 5-7. Results showed varied levels of both increases and decreases of maximum stress in

the pedicles. The largest increases occurred in the L3 during flexion. When the LF was removed during flexion, the maximum stress increased 55%. The majority of the large changes occurred in the L3, while there were some smaller changes that occurred in the L4. The maximum stress in the pedicles of the L2 and L5 remained mostly unchanged.

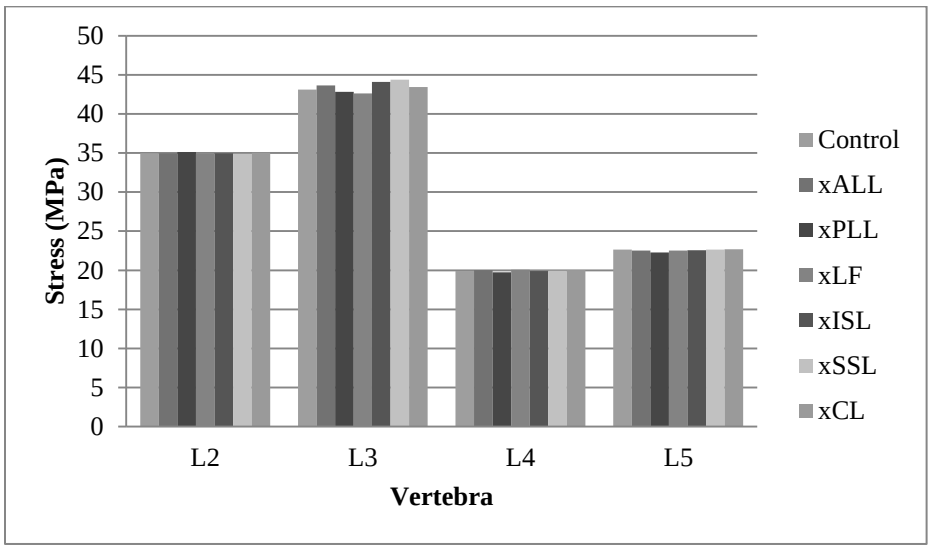

Figure 5-2: Pedicle Stresses During First Axial Rotation

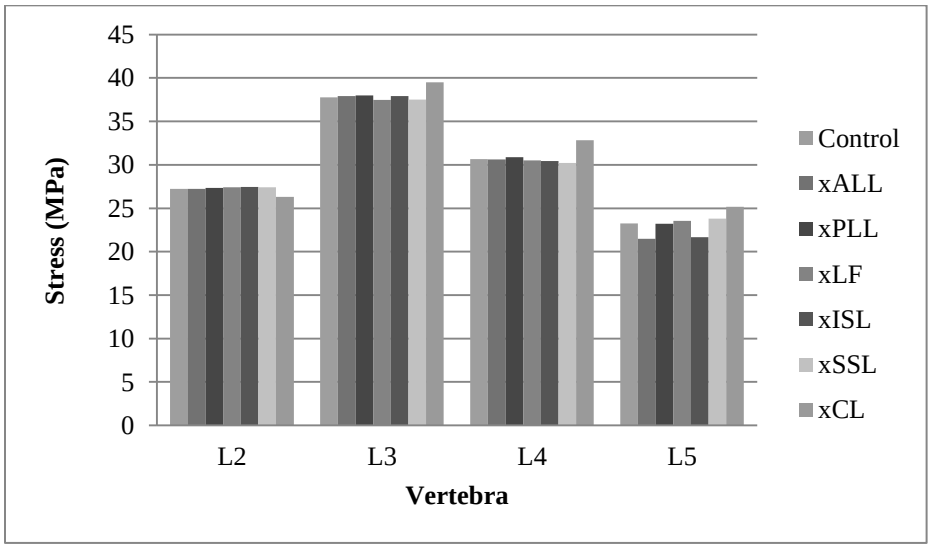

Figure 5-3: Pedicle Stresses During First Axial Rotation

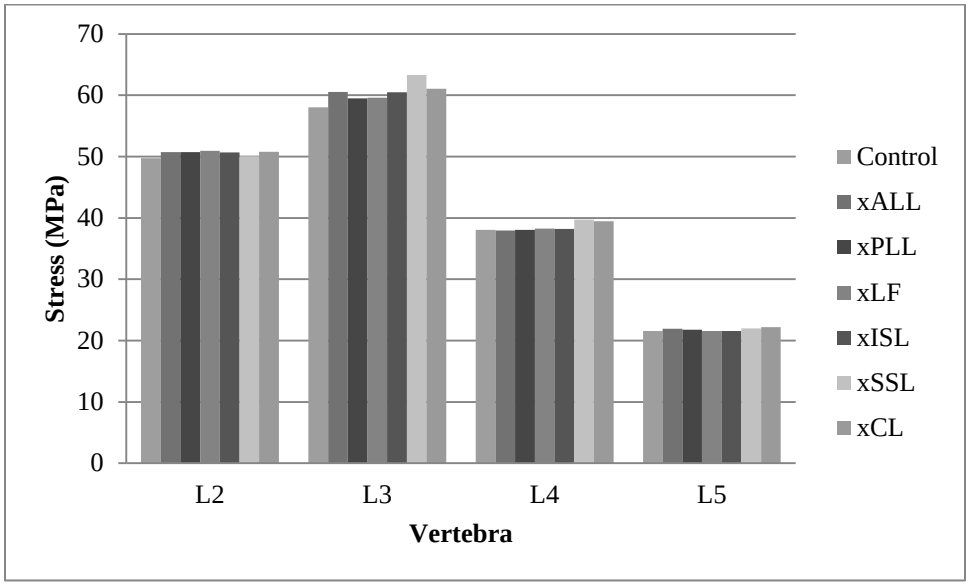

Figure 5-4: Pedicle Stresses During Extension

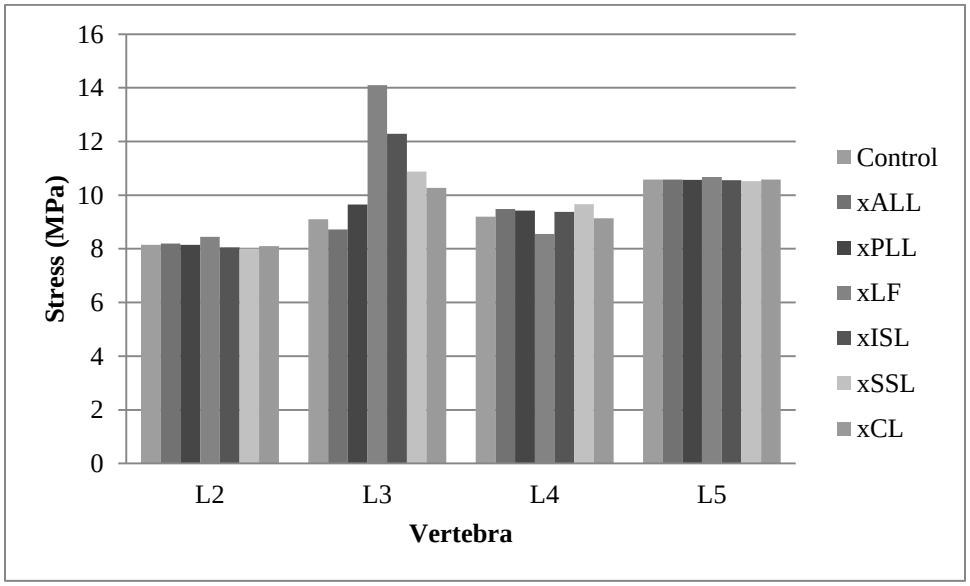

Figure 5-5: Pedicle Stresses During Flexion

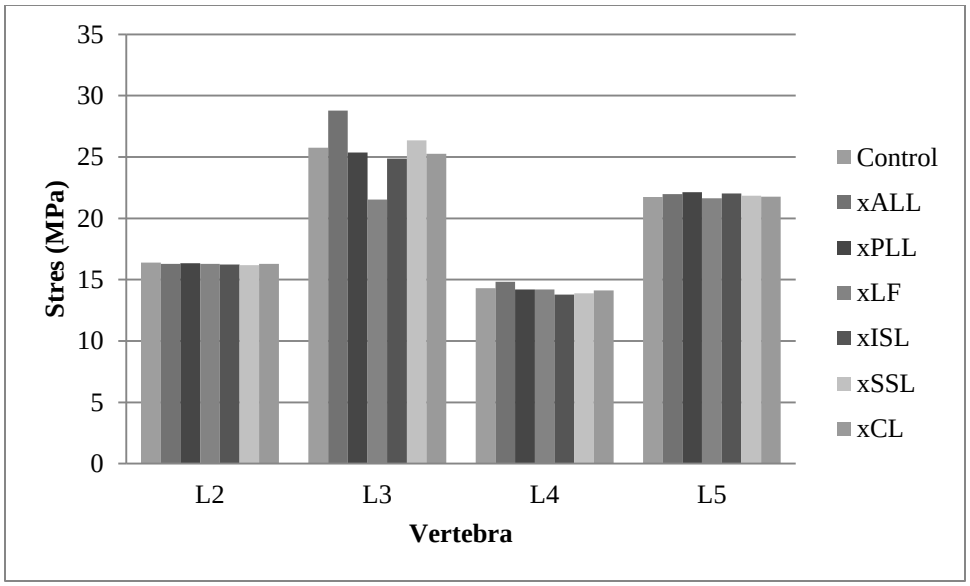

Figure 5-6: Pedicle Stresses During First Lateral Bending

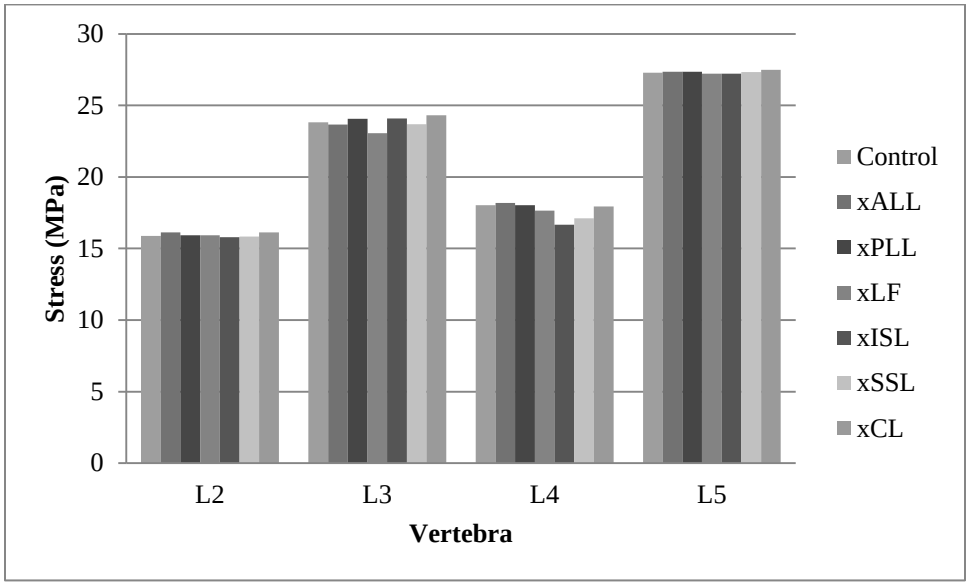

Figure 5-7: Pedicle Stresses During Second Lateral Bending

Figure 5-8 displays how the load was transferred to the remaining elements once a ligament was transected. The load that is carried in the intervertebral discs (around 80%) remained relatively constant and is not included in the figure. The results show that most of the

load not carried by the intervertebral discs is carried in the ISL, SSL, and LF. Therefore, when one of them is removed, the load is transferred to the remaining two ligaments. Also, during extension, the load not carried by the discs is mostly carried by the ALL and the two vertebral bodies. Therefore, if the ALL is removed, the load in the two vertebral bodies increases. The results for both the normal and transverse load sharing for every load case can be found in Appendix B.

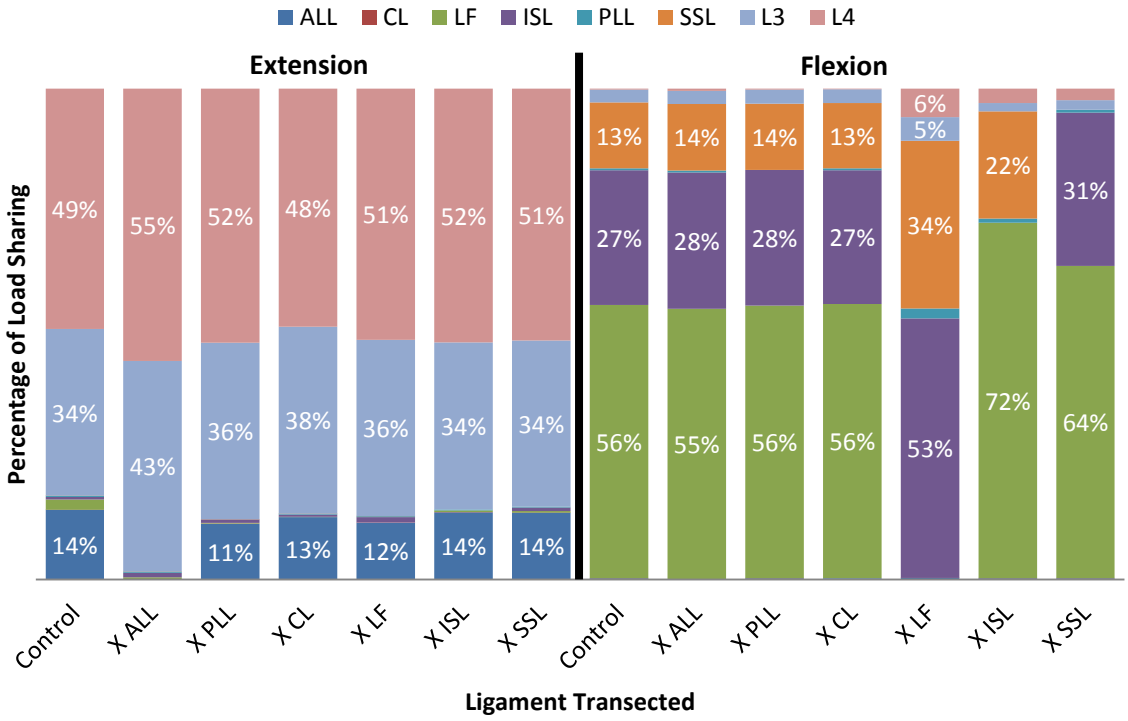

Figure 5-8: Normal Load Sharing Between L3 and L4

5.2 Additional Discussion

The changes in the range of motion as well as the load sharing are consistent with the results already mentioned. The increases in motion during flexion when the ISL, SSL, or LF is removed coincide with the increases in stress in the remaining ligaments. The minimal changes

that occur during axial rotation and lateral bending also support the smaller changes in ligament stress in the remaining ligaments.

The stress increases in the pedicles are also consistent with the strain energy results reported in Chapter 4. The large increase occurred during flexion, and although they may produce changes in bone density, they are still well below cancellous bone failure stresses.

6. SUMMARY AND FUTURE WORK

6.1 Summary

This research shows that changes do occur as a result of ligament transection. Removal of ligaments may lead to damage of the remaining ligaments and cause increases in bone density. Changes are the largest with the removal of a posterior ligament (ISL, SSL, or LF). Larger changes generally occur at the level of the removed ligament and only minimal changes occur at adjacent levels.

This research may be used in the future to help improve the long-term success of spinal surgeries which will ultimately reduce the negative effects of lower back pain. Special attention can be made to any operations that may damage or remove any of the posterior ligaments.

6.2 Future Work

This research showed the large effect that geometry has on modeling the spine. The spine appears to be symmetrical, but slight geometrical differences in the two sides produced asymmetrical biomechanics, especially in left-right lateral bending and left-right axial rotation. It is also possible that the effects of ligament transection could affect the spine of a small boy differently than an adult female. Although patient-specific modeling is currently too time-consuming to allow construction of a finite element model for every patient, it may be beneficial to create a library of finite element models for different types of spines that each patient can better relate to (i.e., a "virtual clinic").

Ligament properties may become more complex in future models. As mentioned in Chapter 4, the results for ligament stress may actually be higher due to the lack of pre-strain. This addition may also help the finite element predictions during extension as the posterior ligaments may still be pulling on the processes at the initial rotations. There is also concurrent research in the BYU Applied Biomechanics Engineering Laboratory that is developing methods for obtaining nonlinear, anisotropic ligament properties. Once those methods are perfected, the resulting ligament material constitutive behavior can be added to the model.

It may also be important to see the effects of removing combinations of ligaments. For example, the ISL and SSL might have redundant functions. The isolated effects of each transection has been shown in this research, but it is unknown how the removal of the SSL after the removal of the ISL will further increase the resulting stresses or if it will have no added effect. This research has clinical relevance, in that more than one ligament is often damaged during spine surgery.

The results also showed possibilities of the increased likelihood of spondylolisthesis. Some ligament removals caused increases in transverse force along the intervertebral disc that may increase the chances of the vertebra slipping out of position. A more extensive analysis is needed to determine these effects.

REFERENCES

1. Katz, J.N., *Lumbar disc disorders and low-back pain: socioeconomic factors and consequences.* J Bone Joint Surg Am, 2006. **88 Suppl 2**: p. 21-4.
2. White, A.P., MM. , *Clinical biomechanics of the spine.* 1990, Lippincott: Philadelphia.
3. Weiss, J.A. and J.C. Gardiner, *Computational modeling of ligament mechanics.* Crit Rev Biomed Eng, 2001. **29**(3): p. 303-71.
4. Woo, S.L., M.A. Gomez, and W.H. Akeson, *The time and history-dependent viscoelastic properties of the canine medical collateral ligament.* J Biomech Eng, 1981. **103**(4): p. 293-8.
5. Schmidt, R., et al., *The impact of implantation technique on frontal and sagittal alignment in total lumbar disc replacement: a comparison of anterior versus oblique implantation.* Eur Spine J, 2010. **19**(9): p. 1534-9.
6. Cakir, B., et al., *Resect or not to resect: the role of posterior longitudinal ligament in lumbar total disc replacement.* Eur Spine J, 2009.
7. Berg, S., *On total disc replacement.* Acta Orthop Suppl, 2011. **82**(343): p. 1-29.
8. Lo, T.P., Jr., S.S. Salerno, and A.R. Colohan, *Interlaminar spacer: a review of its mechanism, application, and efficacy.* World Neurosurg, 2010. **74**(6): p. 617-26.
9. Benzel, E.C. and T. Mroz, *Interlaminar spacers: looks good, smells bad.* World Neurosurg, 2010. **74**(6): p. 576-8.
10. Kim, C.H. and C.K. Chung, *Endoscopic Interlaminar Lumbar Discectomy With Splitting of the Ligament Flavum Under Visual Control.* J Spinal Disord Tech, 2011.
11. Goel, V.K. and L.G. Gilbertson, *Applications of the finite element method to thoracolumbar spinal research--past, present, and future.* Spine (Phila Pa 1976), 1995. **20**(15): p. 1719-27.
12. Goel, V.K. and J.D. Clausen, *Prediction of load sharing among spinal components of a C5-C6 motion segment using the finite element approach.* Spine (Phila Pa 1976), 1998. **23**(6): p. 684-91.
13. Bono, C.M., et al., *Residual sagittal motion after lumbar fusion: a finite element analysis with implications on radiographic flexion-extension criteria.* Spine (Phila Pa 1976), 2007. **32**(4): p. 417-22.
14. Bhattacharya, S., et al., *Models that incorporate spinal structures predict better wear performance of cervical artificial discs.* Spine J, 2011. **11**(8): p. 766-76.
15. Goel, V.K., et al., *Parameters that effect spine biomechanics following cervical disc replacement.* Eur Spine J, 2011.
16. Shirazi-Adl, A., *Nonlinear stress analysis of the whole lumbar spine in torsion--mechanics of facet articulation.* J Biomech, 1994. **27**(3): p. 289-99.

17. Shirazi-Adl, A., *Biomechanics of the lumbar spine in sagittal/lateral moments.* Spine (Phila Pa 1976), 1994. **19**(21): p. 2407-14.
18. Shirazi-Adl, A. and M. Parnianpour, *Load-bearing and stress analysis of the human spine under a novel wrapping compression loading.* Clin Biomech (Bristol, Avon), 2000. **15**(10): p. 718-25.
19. Shirazi-Adl, A., et al., *Muscle force evaluation and the role of posture in human lumbar spine under compression.* Eur Spine J, 2002. **11**(6): p. 519-26.
20. Ng, H.W., E.C. Teo, and Q. Zhang, *Influence of cervical disc degeneration after posterior surgical techniques in combined flexion-extension--a nonlinear analytical study.* J Biomech Eng, 2005. **127**(1): p. 186-92.
21. Ng, H.W. and E.C. Teo, *Influence of preload magnitudes and orientation angles on the cervical biomechanics: a finite element study.* J Spinal Disord Tech, 2005. **18**(1): p. 72-9.
22. Ng, H.W. and E.C. Teo, *Probabilistic design analysis of the influence of material property on the human cervical spine.* J Spinal Disord Tech, 2004. **17**(2): p. 123-33.
23. Rohlmann, A., et al., *Effect of a pedicle-screw-based motion preservation system on lumbar spine biomechanics: a probabilistic finite element study with subsequent sensitivity analysis.* J Biomech, 2010. **43**(15): p. 2963-9.
24. Rohlmann, A., et al., *A probabilistic finite element analysis of the stresses in the augmented vertebral body after vertebroplasty.* Eur Spine J, 2010. **19**(9): p. 1585-95.
25. Dreischarf, M., et al., *A non-optimized follower load path may cause considerable intervertebral rotations.* J Biomech, 2010. **43**(13): p. 2625-8.
26. Dreischarf, M., et al., *Optimised loads for the simulation of axial rotation in the lumbar spine.* J Biomech, 2011. **44**(12): p. 2323-7.
27. Zander, T., G. Bergmann, and A. Rohlmann, *Large sizes of vertebral body replacement do not reduce the contact pressure on adjacent vertebral bodies per se.* Med Eng Phys, 2009. **31**(10): p. 1307-12.
28. Polikeit, A., L.P. Nolte, and S.J. Ferguson, *The effect of cement augmentation on the load transfer in an osteoporotic functional spinal unit: finite-element analysis.* Spine (Phila Pa 1976), 2003. **28**(10): p. 991-6.
29. Polikeit, A., et al., *Factors influencing stresses in the lumbar spine after the insertion of intervertebral cages: finite element analysis.* Eur Spine J, 2003. **12**(4): p. 413-20.
30. Schmidt, H., et al., *Application of a calibration method provides more realistic results for a finite element model of a lumbar spinal segment.* Clin Biomech (Bristol, Avon), 2007. **22**(4): p. 377-84.
31. Schmidt, H., et al., *The risk of disc prolapses with complex loading in different degrees of disc degeneration - a finite element analysis.* Clin Biomech (Bristol, Avon), 2007. **22**(9): p. 988-98.
32. Schmidt, H., F. Heuer, and H.J. Wilke, *Interaction between finite helical axes and facet joint forces under combined loading.* Spine (Phila Pa 1976), 2008. **33**(25): p. 2741-8.
33. Galbusera, F., et al., *Comparison of four methods to simulate swelling in poroelastic finite element models of intervertebral discs.* J Mech Behav Biomed Mater, 2011. **4**(7): p. 1234-41.
34. Schmidt, H., et al., *Response analysis of the lumbar spine during regular daily activities--a finite element analysis.* J Biomech, 2010. **43**(10): p. 1849-56.
35. Bowden, A.E., et al., *Quality of motion considerations in numerical analysis of motion restoring implants of the spine.* Clin Biomech (Bristol, Avon), 2008. **23**(5): p. 536-44.

36. Rundell, S.A., et al., *Total disc replacement positioning affects facet contact forces and vertebral body strains.* Spine (Phila Pa 1976), 2008. **33**(23): p. 2510-7.
37. Rundell, S.A., et al., *Effect of nucleus replacement device properties on lumbar spine mechanics.* Spine (Phila Pa 1976), 2009. **34**(19): p. 2022-32.
38. Womack, W., et al., *Finite element modeling of kinematic and load transmission alterations due to cervical intervertebral disc replacement.* Spine (Phila Pa 1976), 2011. **36**(17): p. E1126-33.
39. Ayturk, U.M. and C.M. Puttlitz, *Parametric convergence sensitivity and validation of a finite element model of the human lumbar spine.* Comput Methods Biomech Biomed Engin, 2011. **14**(8): p. 695-705.
40. Rohlmann, A., T. Zander, and G. Bergmann, *Effect of total disc replacement with ProDisc on intersegmental rotation of the lumbar spine.* Spine (Phila Pa 1976), 2005. **30**(7): p. 738-43.
41. Smith, T., *The Mechanical Significance of the Trabecular Bone Architecture in a Human Vertebra.* Aachen: Shaker, 1996.
42. Panjabi, M.M., et al., *Articular facets of the human spine. Quantitative three-dimensional anatomy.* Spine (Phila Pa 1976), 1993. **18**(10): p. 1298-310.
43. Panjabi, M.M., et al., *Human lumbar vertebrae. Quantitative three-dimensional anatomy.* Spine (Phila Pa 1976), 1992. **17**(3): p. 299-306.
44. Sairyo, K., et al., *Three-dimensional finite element analysis of the pediatric lumbar spine. Part I: pathomechanism of apophyseal bony ring fracture.* Eur Spine J, 2006. **15**(6): p. 923-9.
45. Ulrich, D., et al., *The ability of three-dimensional structural indices to reflect mechanical aspects of trabecular bone.* Bone, 1999. **25**(1): p. 55-60.
46. Morgan, E.F., H.H. Bayraktar, and T.M. Keaveny, *Trabecular bone modulus-density relationships depend on anatomic site.* J Biomech, 2003. **36**(7): p. 897-904.
47. Zander, T., et al., *Estimation of muscle forces in the lumbar spine during upper-body inclination.* Clin Biomech (Bristol, Avon), 2001. **16 Suppl 1**: p. S73-80.
48. Shirazi-Adl, A., et al., *Spinal muscle forces, internal loads and stability in standing under various postures and loads--application of kinematics-based algorithm.* Eur Spine J, 2005. **14**(4): p. 381-92.
49. Patwardhan, A.G., et al., *Effect of compressive follower preload on the flexion-extension response of the human lumbar spine.* J Orthop Res, 2003. **21**(3): p. 540-6.
50. Rohlmann, A., et al., *Comparison of the effects of bilateral posterior dynamic and rigid fixation devices on the loads in the lumbar spine: a finite element analysis.* Eur Spine J, 2007. **16**(8): p. 1223-31.
51. LSTC, *LS-DYNA KEYWORD User's Manual.* 2011. **1**.
52. Chazal, J., et al., *Biomechanical properties of spinal ligaments and a histological study of the supraspinal ligament in traction.* J Biomech, 1985. **18**(3): p. 167-76.
53. Panjabi, M.M., et al., *Mechanical behavior of the human lumbar and lumbosacral spine as shown by three-dimensional load-displacement curves.* J Bone Joint Surg Am, 1994. **76**(3): p. 413-24.
54. Guan, Y., et al., *Validation of a clinical finite element model of the human lumbosacral spine.* Med Biol Eng Comput, 2006. **44**(8): p. 633-41.
55. Frei, H., et al., *The effect of nucleotomy on lumbar spine mechanics in compression and shear loading.* Spine (Phila Pa 1976), 2001. **26**(19): p. 2080-9.

56. Pearcy, M.J. and N. Bogduk, *Instantaneous axes of rotation of the lumbar intervertebral joints.* Spine (Phila Pa 1976), 1988. **13**(9): p. 1033-41.
57. Gillespie, K.A. and J.P. Dickey, *Biomechanical role of lumbar spine ligaments in flexion and extension: determination using a parallel linkage robot and a porcine model.* Spine (Phila Pa 1976), 2004. **29**(11): p. 1208-16.
58. Sharma, M., N.A. Langrana, and J. Rodriguez, *Role of ligaments and facets in lumbar spinal stability.* Spine (Phila Pa 1976), 1995. **20**(8): p. 887-900.
59. Heuer, F., et al., *Stepwise reduction of functional spinal structures increase vertebral translation and intradiscal pressure.* J Biomech, 2007. **40**(4): p. 795-803.
60. Adams, M.A. and W.C. Hutton, *The relevance of torsion to the mechanical derangement of the lumbar spine.* Spine (Phila Pa 1976), 1981. **6**(3): p. 241-8.
61. Panjabi, M.M., V.K. Goel, and K. Takata, *Physiologic strains in the lumbar spinal ligaments. An in vitro biomechanical study 1981 Volvo Award in Biomechanics.* Spine (Phila Pa 1976), 1982. **7**(3): p. 192-203.
62. Zander, T., A. Rohlmann, and G. Bergmann, *Analysis of simulated single ligament transection on the mechanical behaviour of a lumbar functional spinal unit.* Biomed Tech (Berl), 2004. **49**(1-2): p. 27-32.
63. Gudavalli, M.R. and J.J. Triano, *An analytical model of lumbar motion segment in flexion.* J Manipulative Physiol Ther, 1999. **22**(4): p. 201-8.
64. Schmidt, H., et al., *Effect of multilevel lumbar disc arthroplasty on spine kinematics and facet joint loads in flexion and extension: a finite element analysis.* Eur Spine J, 2010.
65. Khoo, L.T., et al., *Minimally invasive percutaneous posterior lumbar interbody fusion.* Neurosurgery, 2002. **51**(5 Suppl): p. S166-1.
66. Voor, M.J., et al., *Biomechanical evaluation of posterior and anterior lumbar interbody fusion techniques.* J Spinal Disord, 1998. **11**(4): p. 328-34.
67. Song, J. and Y. Park, *Ligament-sparing lumbar microdiscectomy: technical note.* Surg Neurol, 2000. **53**(6): p. 592-6; discussion 596-7.
68. Bowden, A.E., *Finite element modeling of the spine*, in *Spine Technology Handbook*, S.M. Kurtz and A.A. Edidin, Editors. 2006, Elsevier Academic Press: London.
69. Lee, C.K., et al., *Impact response of the intervertebral disc in a finite-element model.* Spine, 2000. **25**(19): p. 2431-9.
70. Goel, V.K., et al., *Interlaminar shear stresses and laminae separation in a disc. Finite element analysis of the L3-L4 motion segment subjected to axial compressive loads.* Spine (Phila Pa 1976), 1995. **20**(6): p. 689-98.
71. Noailly, J., D. Lacroix, and J.A. Planell, *Finite element study of a novel intervertebral disc substitute.* Spine (Phila Pa 1976), 2005. **30**(20): p. 2257-64.
72. Elliott, D.M. and L.A. Setton, *Anisotropic and inhomogeneous tensile behavior of the human anulus fibrosus: experimental measurement and material model predictions.* J Biomech Eng, 2001. **123**(3): p. 256-63.
73. Sairyo, K., et al., *Three dimensional finite element analysis of the pediatric lumbar spine. Part II: biomechanical change as the initiating factor for pediatric isthmic spondylolisthesis at the growth plate.* Eur Spine J, 2006. **15**(6): p. 930-5.
74. Sizer, P.S., Jr., V. Phelps, and O. Matthijs, *Pain generators of the lumbar spine.* Pain Pract, 2001. **1**(3): p. 255-73.
75. Little, J.S. and P.S. Khalsa, *Material properties of the human lumbar facet joint capsule.* J Biomech Eng, 2005. **127**(1): p. 15-24.

76. Huiskes, R., et al., *Adaptive bone-remodeling theory applied to prosthetic-design analysis.* J Biomech, 1987. **20**(11-12): p. 1135-50.
77. Fyhrie, D.P. and D.R. Carter, *A unifying principle relating stress to trabecular bone morphology.* J Orthop Res, 1986. **4**(3): p. 304-17.
78. Tomaszewski, P.K., et al., *A comparative finite-element analysis of bone failure and load transfer of osseointegrated prostheses fixations.* Ann Biomed Eng, 2010. **38**(7): p. 2418-27.
79. Bougherara, H., M.N. Bureau, and L. Yahia, *Bone remodeling in a new biomimetic polymer-composite hip stem.* J Biomed Mater Res A, 2010. **92**(1): p. 164-74.
80. Viceconti, M., et al., *Extracting clinically relevant data from finite element simulations.* Clin Biomech (Bristol, Avon), 2005. **20**(5): p. 451-4.

APPENDIX A. DISC PRESSURE RESULTS

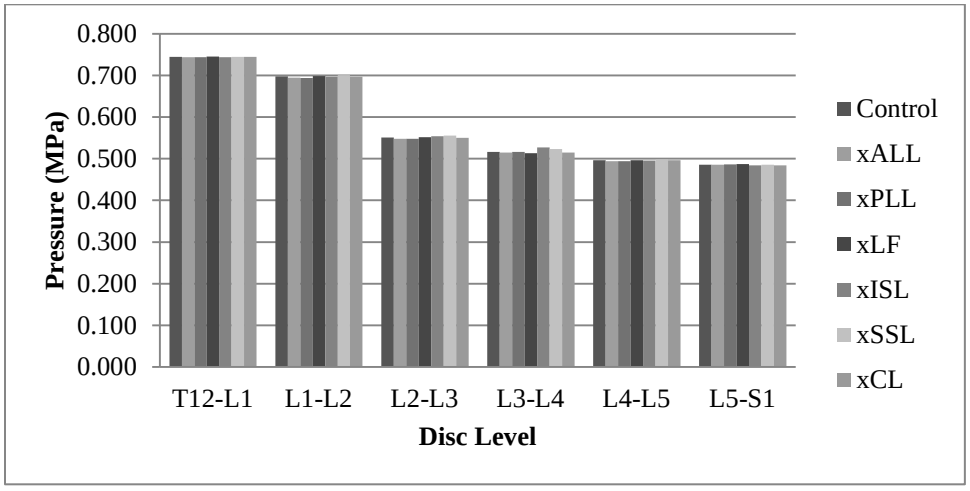

Figure A-1: Disc Pressure During First Axial Rotation

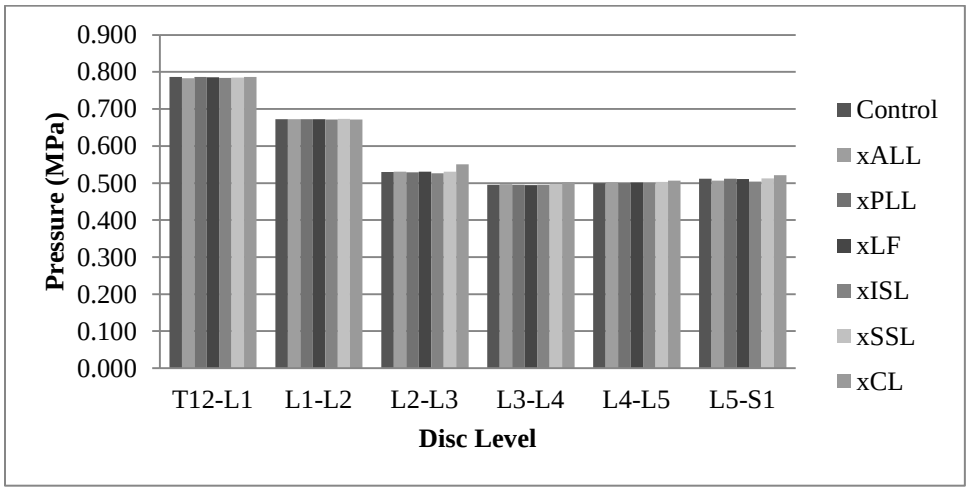

Figure A-2: Disc Pressure During Second Axial Rotation

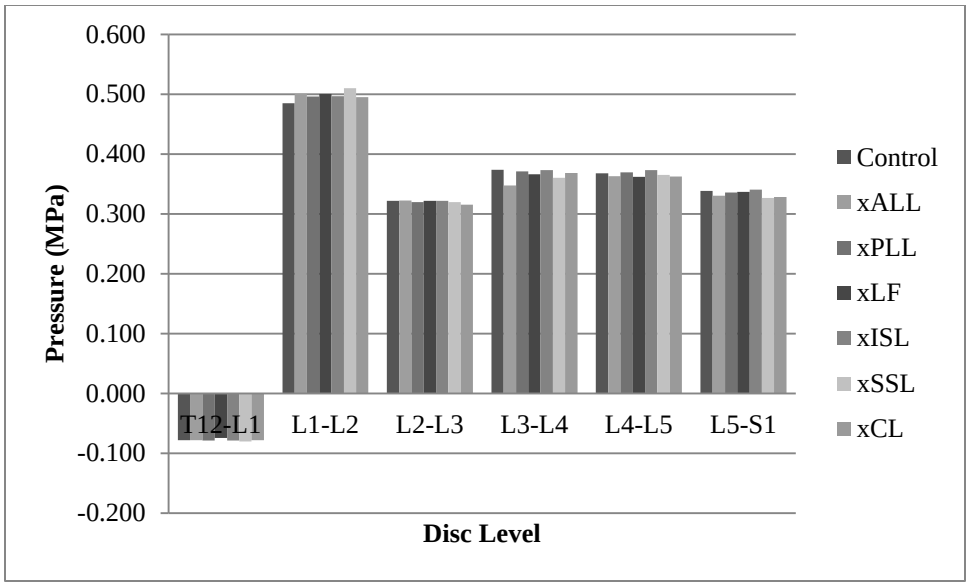

Figure A-3: Disc Pressure During Extension

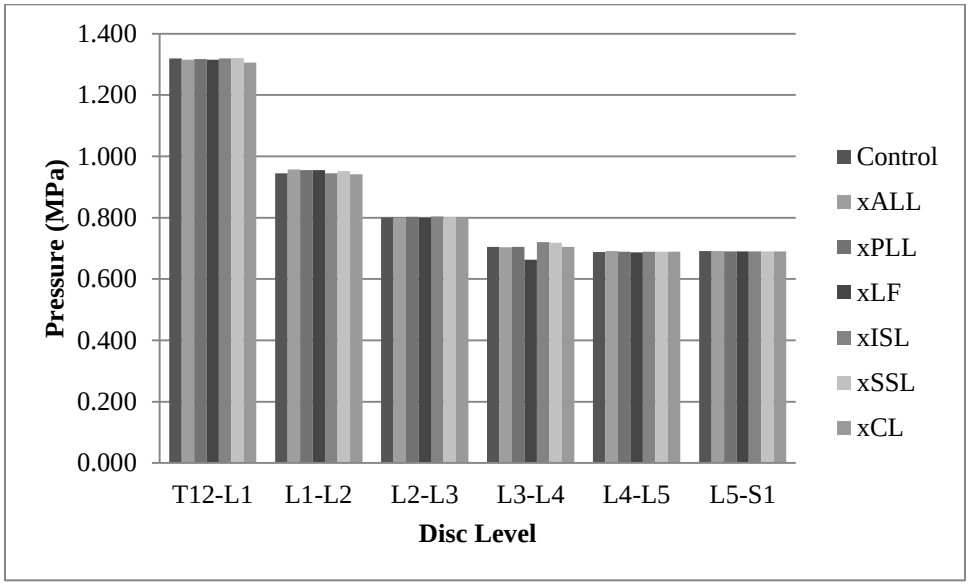

Figure A-4: Disc Pressure During Flexion

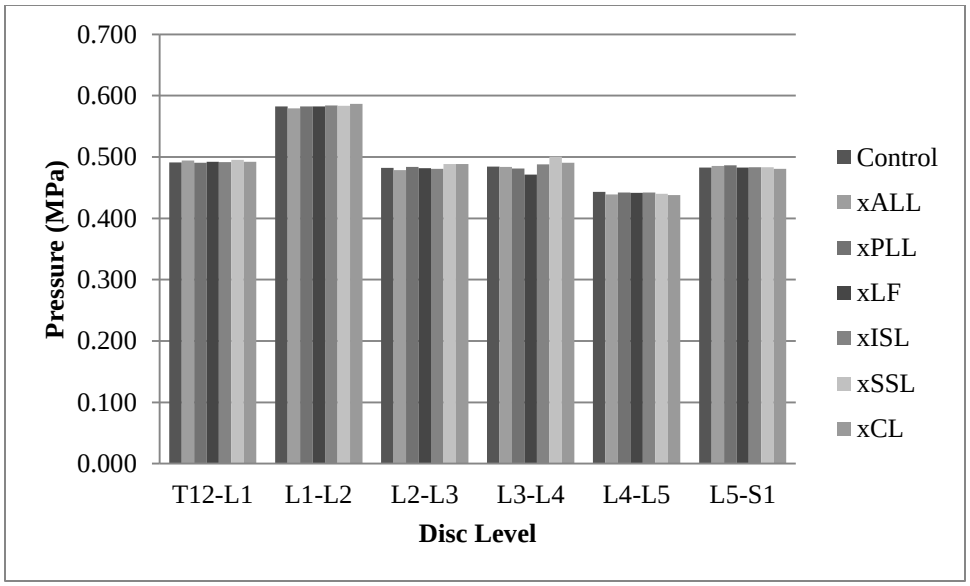

Figure A-5: Disc Pressure During First Lateral Bending

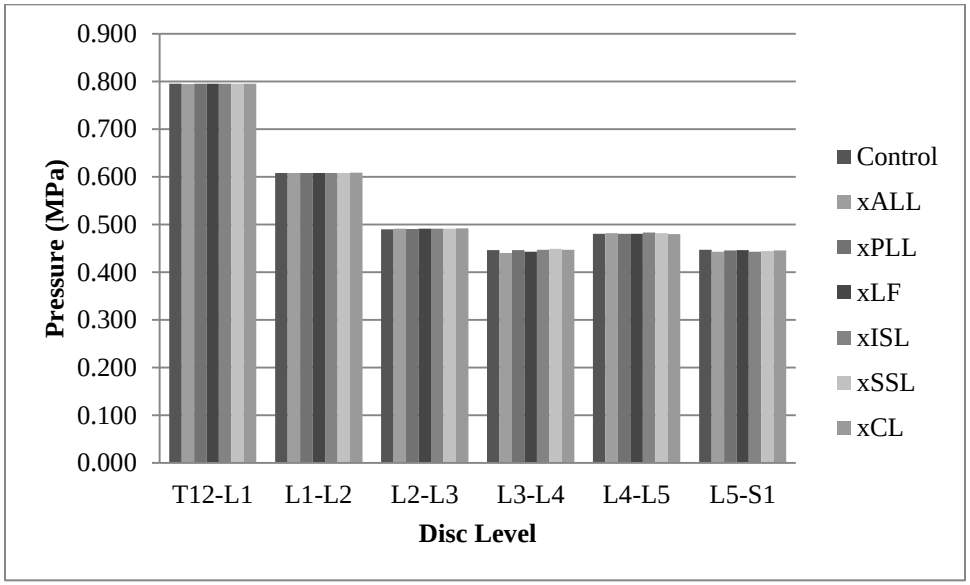

Figure A-6: Disc Pressure During Second Lateral Bending

APPENDIX B. LOAD SHARING RESULTS

Table B-1: Normal Load Forces in First Axial Rotation

		Control	ALL	PLL	LF	ISL	SSL	CL
	Disc	-418.498	-416.446	-416.225	-418.992	-418.081	-420.645	-418.169
	ALL	1.27957	1.29682	1.27869	1.2681	1.26531	1.25641	1.27579
	CL	0.009454	0.009444	0.009496	0.00947	0.009477	0.009453	0.009476
LEVEL 1 (L1-L2)	FL	11.2494	11.0028	11.0768	11.1329	11.2372	11.5475	11.2991
	ISL	8.62866	8.55597	8.57119	8.60631	8.67721	8.68489	8.67717
	PLL	0.016047	0.01601	0.016021	0.016224	0.015749	0.016857	0.01676
	SSL	6.99979	6.89017	6.94276	7.02785	6.99825	7.11031	7.00521
	L1	-6.22008	-6.21301	-6.23069	-6.22532	-6.16492	-6.17741	-6.20759
	L2	4.85636	4.78081	4.73895	5.02505	5.14256	5.27982	4.91776
	Disc	-442.452	-439.757	-439.572	-442.86	-443.397	-444.877	-441.642
	ALL	1.38253	1.38734	1.39391	1.37095	1.33726	1.33582	1.38677
	CL	0.027088	0.027003	0.027136	0.027072	0.027005	0.027086	0.027215
LEVEL 2 (L2-L3)	FL	18.2866	18.4888	18.4487	18.1487	18.7974	18.892	18.3522
	ISL	16.8117	16.7961	16.7791	16.8138	16.8443	16.9357	16.8161
	PLL	0.085864	0.083694	0.088102	0.083118	0.084414	0.08383	0.084913
	SSL	6.39752	6.39612	6.31055	6.42811	6.38965	6.47641	6.39121
	L2	-8.19707	-8.37451	-8.31707	-8.1333	-8.16128	-8.17952	-8.18123
	L3	9.36132	9.59551	9.91462	8.80757	11.0932	9.35815	9.53352
	Disc	-433.215	-431.353	-434.082	-428.013	-437.21	-438.229	-432.339
	ALL	-0.10743	0	-0.09772	-0.11867	-0.1382	-0.11664	-0.10682
	CL	0.015085	0.014489	0.014671	0.016823	0.022601	0.016842	0
LEVEL 3 (L3-L4)	FL	9.22413	10.7952	9.9699	0	21.3094	12.9036	9.47249
	ISL	15.3075	15.2849	15.0078	17.7638	0	17.085	15.5795
	PLL	-0.0733	-0.07367	0	-0.06679	-0.06733	-0.07198	-0.07301
	SSL	6.32487	6.31425	6.2363	7.26391	7.94099	0	6.42295
	L3	0.401925	0.578573	0.188687	0.549199	-0.5459	-0.02835	0.417407
	L4	10.0107	9.91982	8.67488	9.37883	4.73161	7.63329	8.54677
	Disc	-411.528	-409.903	-409.735	-412.102	-411.3	-412.547	-411.404
	ALL	0.847278	0.850999	0.859764	0.849734	0.847479	0.834605	0.847541
	CL	0.064813	0.065252	0.064531	0.064525	0.064271	0.063884	0.064201
LEVEL 4 (L4-L5)	FL	0.796545	0.934786	1.22011	0.902542	0.874635	0.765013	1.20199
	ISL	18.3339	18.4471	18.3844	18.2677	18.442	18.2491	18.3343
	PLL	0.01896	0.018539	0.018149	0.0182	0.017887	0.01851	0.018128
	SSL	7.37819	7.94825	7.97786	7.35946	8.15093	7.49841	8.07664
	L4	-1.45241	-1.38982	-1.45601	-1.56203	-1.14903	-0.8841	-1.34683
	L5	-13.0434	-13.4052	-13.3749	-13.4948	-12.2695	-13.7697	-12.2636

Results are in N

Table B-2: Normal Load Forces in Second Axial Rotation

		Control	ALL	PLL	LF	ISL	SSL	CL
	Disc	-407.29	-406.672	-407.228	-407.131	-406.166	-407.324	-406.061
	ALL	0.576162	0.546091	0.606826	0.572666	0.548222	0.556759	0.493468
	CL	0.013344	0.012894	0.013509	0.013305	0.013234	0.013094	0.012112
LEVEL 1 (L1-L2)	FL	12.1166	11.7932	12.0348	12.2109	12.2391	12.1389	14.7355
	ISL	6.60194	6.44195	6.53434	6.56799	6.67261	6.52485	6.84426
	PLL	0.094459	0.092387	0.094029	0.093496	0.09299	0.095586	0.093896
	SSL	8.3648	8.35817	8.34407	8.40805	8.47462	8.40115	9.06444
	L1	8.93074	8.88131	8.95112	8.95713	9.03039	8.92049	9.2206
	L2	15.8306	15.673	15.9098	15.7623	15.754	15.685	14.5419
	Disc	-420.666	-421.034	-420.558	-420.381	-418.228	-420.786	-434.928
	ALL	0.373532	0.374523	0.381304	0.364669	0.380133	0.353113	0.345094
	CL	0.012193	0.012025	0.012135	0.012232	0.012113	0.012227	0.012968
LEVEL 2 (L2-L3)	FL	2.28407	2.45642	1.75224	2.5306	2.43108	2.20212	1.81375
	ISL	6.25838	6.17575	6.12467	6.46931	6.11805	6.58452	6.71719
	PLL	0.137873	0.138912	0.137852	0.137212	0.134957	0.137304	0.135812
	SSL	3.2603	3.21159	3.18955	3.40168	3.15464	3.44285	3.15592
	L2	-1.77378	-1.77025	-2.0732	-1.64784	-1.88347	-1.49691	-1.74553
	L3	8.69037	8.85516	9.00257	8.47271	8.99903	8.64981	8.21576
	Disc	-416.361	-417.482	-416.488	-414.857	-412.866	-415.622	-433.783
	ALL	-0.11908	0	-0.11749	-0.12934	-0.14935	-0.15542	-0.15202
	CL	0.008633	0.008414	0.008674	0.008569	0.007737	0.007385	0
LEVEL 3 (L3-L4)	FL	0.847669	1.16415	2.11302	0	2.71022	2.00683	5.58859
	ISL	8.18203	7.79393	8.15873	8.76381	0	10.7695	5.96708
	PLL	-0.02217	-0.0223	0	-0.01901	-0.00752	-0.00977	-0.05061
	SSL	3.51013	3.37584	3.49581	3.83243	4.83116	0	2.19917
	L3	3.77679	3.48576	3.68367	3.5907	2.26779	2.46124	3.82029
	L4	30.1785	30.1382	29.8446	30.1607	28.84	28.6367	29.704
	Disc	-406.076	-408.533	-405.201	-406.868	-405.866	-408.18	-408.433
	ALL	-0.44427	-0.45164	-0.45811	-0.45486	-0.41701	-0.46256	-0.39915
	CL	0.033877	0.033288	0.033926	0.033699	0.033825	0.033586	0.030988
LEVEL 4 (L4-L5)	FL	1.81923	1.18466	2.33743	1.8367	1.43608	1.63135	1.32944
	ISL	12.3833	11.9243	12.6549	12.4039	11.9677	12.2978	10.8816
	PLL	0.056184	0.053761	0.056525	0.056384	0.055938	0.056491	0.04346
	SSL	8.32337	8.22462	8.68147	8.44423	7.91291	8.34526	7.64005
	L4	4.26085	3.69133	4.75879	4.59044	3.68922	4.86188	5.06116
	L5	49.159	46.3404	50.1978	50.7124	46.8364	51.2321	55.9395

Results are in N

Table B-3: Normal Load Forces in Extension

		Control	ALL	PLL	LF	ISL	SSL	CL
	Disc	-298.295	-308.412	-305.355	306.807	-307.857	-313.493	-304.774
	ALL	3.14508	3.13385	3.24927	3.45894	3.1709	2.88843	3.27871
	CL	0.001592	0.001525	0.001524	0.002923	0.001565	0.00267	0.001502
LEVEL 1 (L1-L2)	FL	0.598829	2.47085	0.287439	0.322892	0.570439	-0.03118	0.218684
	ISL	-0.00675	-0.00447	-0.00345	0.032476	0.006711	0.009672	-0.0003
	PLL	0.028446	0.036316	0.034873	0.155585	0.034599	0.053698	0.038542
	SSL	0.001337	9.89E-05	-0.00042	0.000526	0.000475	0.001714	0.000462
	L1	-11.8082	-12.9419	-13.6639	29.4566	-13.1623	-12.7477	-12.9502
	L2	5.89389	5.56585	6.08508	27.2798	6.00495	3.03822	5.79998
	Disc	-368.889	-368.196	-366.629	375.494	-367.359	-366.249	-364.998
	ALL	11.0421	10.8117	11.4001	11.4514	10.906	11.6901	11.67
	CL	0.006639	0.007971	0.008057	0.016222	0.006809	0.008006	0.007236
LEVEL 2 (L2-L3)	FL	0.816289	0.09168	0.131878	0.18483	0.796156	0.414419	0.557263
	ISL	0.26001	0.265971	0.464411	0.618003	0.299774	0.054738	0.337744
	PLL	0.190365	0.186067	0.189579	0.619751	0.183925	0.199593	0.194989
	SSL	0.000752	-0.00371	-0.00022	0.00023	-8.6E-05	0.000361	-6.9E-05
	L2	-54.0508	-51.2135	-51.1098	67.4742	-47.7458	-56.6335	-55.297
	L3	17.1985	16.0677	16.2721	30.7755	17.2371	15.0417	14.1354
	Disc	-386.492	-357.606	-374.611	388.895	-370.807	-371.024	-376.377
	ALL	12.828	0	10.0032	10.4844	10.5363	12.3546	11.5464
	CL	0.023757	0.022297	0.020921	0.025245	0.02133	0.023468	0
LEVEL 3 (L3-L4)	FL	1.87974	0.34859	0.148525	0.183985	0	0.29506	0.037779
	ISL	0.458454	0.697332	0.621058	0.792332	1.00627	0.64131	0.433323
	PLL	-0.22702	-0.20717	0	0	-0.19713	-0.20292	-0.2062
	SSL	-0.0002	-8.4E-05	0.00026	0.000675	0.000983	0	0.000193
	L3	-30.6808	-33.3519	-31.6687	56.878	-32.691	-30.6783	-34.5724
	L4	44.2015	43.0955	45.4796	49.1144	46.5518	46.5719	44.0063
	Disc	-344.532	-339.201	-345.163	373.875	-339.569	-342.053	-339.799
	ALL	10.0269	10.6921	10.2744	10.6338	10.5431	11.0258	11.1898
	CL	0.031811	0.032574	0.032198	0.035614	0.032429	0.031233	0.033441
LEVEL 4 (L4-L5)	FL	0.237817	0.243213	0.216185	0.227287	0.208881	0.137412	0.219167
	ISL	0.477599	0.523802	0.516646	0.699775	0.610514	0.744113	0.539285
	PLL	0.092293	0.095116	0.091656	0.194056	0.095001	0.085662	0.09911
	SSL	-0.00067	-0.00053	0.000319	0.000589	0.000294	-0.0013	-1.5E-05
	L4	-33.0856	-34.4081	-34.8587	44.1099	-34.315	-36.2604	-34.4223
	L5	11.9031	16.1859	17.1799	27.5306	14.2585	16.2079	15.6722

Results are in N

Table B-4: Normal Load Forces in Flexion

		Control	ALL	PLL	LF	ISL	SSL	CL
	Disc	-582.83	-583.785	-585.101	-585.715	-582.222	-583.342	-583.243
	ALL	-0.19426	-0.19289	-0.18963	-0.19259	-0.18927	-0.1919	-0.19247
	CL	0.008271	0.008137	0.008116	0.00815	0.008065	0.008108	0.008267
LEVEL 1 (L1-L2)	FL	78.6797	78.4254	78.5607	79.0888	79.1371	79.4408	79.2365
	ISL	23.0522	22.9724	23.1315	23.1603	23.1126	23.0791	23.1521
	PLL	0.628106	0.604855	0.618728	0.629197	0.634559	0.616798	0.62282
	SSL	24.2306	24.1352	24.3649	24.3096	24.2382	24.2736	24.3405
	L1	-2.30794	1.27888	5.16644	0.743198	2.05361	1.17233	2.36893
	L2	2.86837	2.87146	3.91511	2.89851	2.68108	3.45656	3.08222
	Disc	-602.832	-601.326	-603.254	-601.885	-603.293	-603.7	-602.697
	ALL	0.211136	0.208273	0.208808	0.209181	0.211865	0.210637	0.208444
	CL	0.00643	0.006397	0.006404	0.006176	0.006237	0.006311	0.006401
LEVEL 2 (L2-L3)	FL	92.6446	92.4407	92.667	90.8496	92.5731	92.7635	92.1529
	ISL	34.0599	34.0343	34.1115	34.4859	33.8671	33.721	34.0447
	PLL	0.474744	0.461211	0.473776	0.422902	0.469969	0.482564	0.458764
	SSL	15.681	15.6149	15.6589	16.1769	15.4557	15.4195	15.5988
	L2	1.5346	1.3464	1.21804	1.32481	1.37703	1.35345	1.2654
	L3	1.99873	1.9881	1.73794	-2.5958	3.08477	3.16728	1.33722
	Disc	-586.921	-586.463	-587.071	-543.235	-595.487	-597.166	-587.337
	ALL	-0.32566	0	-0.32529	-0.3039	-0.33961	-0.33581	-0.32743
	CL	0.005731	0.005645	0.00571	0.010473	0.009425	0.008165	0
LEVEL 3 (L3-L4)	FL	76.1002	74.0361	74.9188	0	105.006	91.4524	77.0099
	ISL	37.4946	37.2626	37.2946	51.4319	0	44.7907	37.5711
	PLL	0.536162	0.526597	0	2.00731	1.23614	0.869544	0.551968
	SSL	18.2902	18.1696	18.2163	33.2084	31.6955	0	18.3255
	L3	3.58259	3.5624	3.78869	4.70324	2.42942	2.78491	3.83266
	L4	0.246298	0.600537	0.264133	5.60322	-4.20227	-3.37162	-0.14901
	Disc	-576.015	-577.618	-576.232	-575.04	-576.323	-576.39	-576.315
	ALL	-0.30006	-0.30109	-0.30055	-0.30385	-0.29554	-0.29985	-0.30085
	CL	0.019747	0.01971	0.019783	0.020215	0.019453	0.019477	0.01983
LEVEL 4 (L4-L5)	FL	70.1964	70.0525	70.0512	68.2683	70.5418	70.9152	69.9722
	ISL	22.5413	22.4312	22.5877	22.7997	22.3883	22.324	22.563
	PLL	0.271422	0.266651	0.270607	0.263669	0.271572	0.279936	0.267968
	SSL	42.3478	42.3365	42.4887	43.1366	42.0734	41.8989	42.4547
	L4	2.34281	2.54402	2.37312	0.710325	2.84464	3.31568	2.31276
	L5	-2.9903	-2.49538	-3.2358	-2.10515	-3.45151	-3.37756	-3.28234

Results are in N

Table B-5: Normal Load Forces in First Lateral Bending

		Control	ALL	PLL	LF	ISL	SSL	CL
	Disc	-415.122	-412.921	-415.334	-415.012	-416.804	-415.923	-417.63
	ALL	6.33061	6.39837	6.35524	6.34545	6.28939	6.38388	6.26473
	CL	0.012085	0.012079	0.012198	0.012184	0.012223	0.012132	0.012041
LEVEL 1 (L1-L2)	FL	22.8476	22.7753	23.0274	22.5644	23.277	22.5106	22.416
	ISL	4.00769	3.99249	4.07352	4.06842	4.19467	3.951	3.97368
	PLL	0.323326	0.319907	0.328027	0.321566	0.324401	0.317158	0.320962
	SSL	6.7397	6.69373	6.85119	6.71615	6.8846	6.74868	6.72989
	L1	10.1496	10.4425	10.664	10.0784	10.1324	10.3224	10.1853
	L2	-10.3396	-10.2289	-10.3772	-10.7143	-10.3939	-10.5664	-10.4225

	Disc	-450.502	-448.242	-450.932	-450.523	-450.31	-455.235	-455.179
	ALL	5.70116	5.66714	5.73361	5.73179	5.71579	5.58254	5.60392
	CL	0.011654	0.011851	0.01167	0.011611	0.011611	0.011767	0.01185
LEVEL 2 (L2-L3)	FL	26.6186	27.331	26.4216	26.2394	26.4313	27.3234	26.9772
	ISL	7.59288	7.66465	7.70446	7.85862	7.71193	7.79712	7.76447
	PLL	0.365655	0.380254	0.369167	0.352811	0.362229	0.38111	0.373806
	SSL	4.1833	4.21916	4.15055	4.26366	4.11816	4.29447	4.31687
	L2	1.8149	1.86565	1.98583	1.87616	1.94952	2.05986	1.95281
	L3	-4.27642	-7.55605	-4.05512	-6.52942	-3.66611	-2.64176	-3.61918

	Disc	-437.33	-436.106	-434.618	-425.073	-440.931	-447.36	-441.951
	ALL	4.4554	0	4.47713	4.57459	4.39473	4.39206	4.40058
	CL	0.020194	0.02219	0.020366	0.020008	0.020183	0.021677	0
LEVEL 3 (L3-L4)	FL	28.8595	31.0954	30.2716	0	35.5771	30.6156	27.8007
	ISL	12.6135	12.3793	12.7477	16.3186	0	13.6919	12.7009
	PLL	1.32919	1.27489	0	1.96025	1.54354	1.3726	1.33154
	SSL	6.54919	6.37004	6.60275	8.20912	7.47979	0	6.58017
	L3	-4.3799	-3.63215	-4.26836	-1.12641	-3.0104	-3.28268	-4.545
	L4	-10.0369	-11.8599	-9.85414	-10.1016	-11.4772	-11.1678	-11.6294

	Disc	-415.325	-412.921	-414.185	-414.264	-413.973	-414.627	-411.634
	ALL	3.31196	3.30148	3.35552	3.29616	3.29392	3.28639	3.32612
	CL	0.026219	0.026138	0.026263	0.026132	0.025753	0.025724	0.026236
LEVEL 4 (L4-L5)	FL	11.7895	13.0496	12.0756	12.1559	11.4405	12.3331	12.1901
	ISL	10.5359	10.714	10.5294	10.5153	10.175	10.3787	10.6023
	PLL	0.734334	0.756372	0.7365	0.730157	0.713007	0.738191	0.746319
	SSL	13.3788	13.6251	13.2572	13.3072	12.8567	13.2222	13.3405
	L4	0.367065	0.961332	0.646181	0.659798	1.22805	1.70196	1.02759
	L5	-26.3514	-25.566	-27.6241	-26.0024	-27.5231	-27.0462	-25.136

Results are in N

Table B-6: Normal Load Forces in Second Lateral Bending

		Control	ALL	PLL	LF	ISL	SSL	CL
	Disc	-441.527	-441.315	-441.588	-441.693	-441.835	-441.406	-442.163
	ALL	4.02614	4.02085	4.0218	4.02509	4.0331	4.02623	4.01125
	CL	0.010241	0.010274	0.010243	0.010245	0.010212	0.010247	0.01027
LEVEL 1 (L1-L2)	FL	11.8907	11.8939	11.8004	11.8963	11.8038	11.9353	11.9526
	ISL	0.780794	0.792065	0.783177	0.779473	0.773565	0.795906	0.804067
	PLL	0.355061	0.357976	0.354684	0.358355	0.356079	0.360159	0.358056
	SSL	2.44426	2.45278	2.44753	2.47174	2.44669	2.47615	2.48699
	L1	-1.3188	-1.31492	-1.32298	-1.30562	-1.31995	-1.30841	-1.32245
	L2	7.50351	7.60863	7.41463	7.58575	7.5219	7.37667	7.42461

	Disc	-455.035	-456.188	-455.301	-455.67	-455.736	-455.421	-456.439
	ALL	6.6774	6.67762	6.66122	6.66099	6.65623	6.65469	6.65919
	CL	0.006485	0.00647	0.006442	0.006455	0.003591	0.003555	0.003578
LEVEL 2 (L2-L3)	FL	10.5291	11.688	11.5032	11.157	10.712	11.0369	11.2225
	ISL	1.46614	1.43016	1.50384	1.48922	1.41026	1.49047	1.45492
	PLL	0.133027	0.12983	0.131444	0.130364	0.130011	0.133224	0.131047
	SSL	1.52567	1.47738	1.52388	1.55404	1.48644	1.53662	1.52758
	L2	-4.73931	-5.07953	-4.76106	-4.8347	-4.87558	-4.81446	-4.8991
	L3	3.68219	3.90827	3.41598	3.3078	4.42993	4.05087	3.86626

	Disc	-430.971	-426.066	-430.846	-427.626	-431.884	-433.079	-431.991
	ALL	2.77176	0	2.7703	2.71159	2.56725	2.61868	2.783
	CL	0.010568	0.01074	0.010567	0.010418	0.010864	0.010639	0
LEVEL 3 (L3-L4)	FL	6.80289	6.74949	6.46605	0	11.8418	9.59769	6.52829
	ISL	11.8898	11.5885	11.8091	13.2493	0	14.0309	11.7133
	PLL	0.050395	0.045276	0	0.103314	0.17694	0.099658	0.044147
	SSL	5.61516	5.46242	5.58262	6.2223	7.00184	0	5.51075
	L3	-5.51733	-5.60534	-5.49676	-4.96923	-5.60307	-5.32212	-5.47395
	L4	1.00219	0.345026	0.948526	1.25101	0.527073	-0.24781	0.555246

	Disc	-433.311	-433.129	-432.991	-433.08	-433.935	-433.506	-432.865
	ALL	5.75065	5.74387	5.74561	5.72366	5.69784	5.70969	5.7461
	CL	0.026086	0.026017	0.026056	0.025931	0.025705	0.025799	0.026023
LEVEL 4 (L4-L5)	FL	6.21737	6.47724	6.37038	6.35982	6.36539	6.52407	6.49098
	ISL	5.0559	5.09716	5.08354	5.07588	4.97914	5.02575	5.11699
	PLL	0.002423	0.00269	0.002821	0.002596	0.002805	0.002688	0.002681
	SSL	2.19384	2.27405	2.25137	2.25322	2.09941	2.15386	2.30566
	L4	-3.21192	-3.06035	-3.15321	-3.13778	-2.99313	-2.78219	-3.0916
	L5	-8.45133	-8.41273	-8.67864	-8.86907	-7.72743	-8.17391	-8.53963

Results are in N

Table B-7: Transverse Load Forces in First Axial Rotation

		Control	ALL	PLL	LF	ISL	SSL	CL
	Disc	75.0105	74.8044	74.4295	74.9877	74.946	75.0713	74.8738
	ALL	3.01607	3.02578	3.00404	3.01177	3.01348	3.00599	3.01296
	CL	0.006824	0.006805	0.00684	0.006823	0.006808	0.006827	0.006836
LEVEL 1 (L1-L2)	FL	1.06026	1.05358	1.02515	1.02979	1.03191	1.06312	1.04953
	ISL	1.92804	1.94361	1.93905	1.9409	1.98435	1.94445	1.9801
	PLL	0.197145	0.197571	0.19488	0.197124	0.19635	0.19884	0.197376
	SSL	1.05327	1.03512	1.0373	1.05989	1.04833	1.06822	1.05377
	L1	19.9752	19.861	19.9136	20.022	20.0432	20.0123	19.97
	L2	9.65251	9.66592	9.866	9.54885	9.37817	9.48387	9.70686

	Disc	90.8062	90.7323	90.7221	90.6916	90.6466	90.6941	90.751
	ALL	2.59982	2.61367	2.61191	2.59055	2.5736	2.57267	2.60667
	CL	0.020019	0.019964	0.020025	0.020031	0.019933	0.019922	0.020064
LEVEL 2 (L2-L3)	FL	0.766692	0.789868	0.791843	0.731198	0.75391	0.748627	0.766059
	ISL	4.66431	4.66589	4.67561	4.66846	4.6834	4.69447	4.67828
	PLL	0.154523	0.150318	0.153392	0.154756	0.152866	0.150905	0.15271
	SSL	1.9165	1.93006	2.17767	1.92473	1.91999	1.92772	1.91925
	L2	32.0652	32.2718	32.1479	32.1914	32.3561	32.1428	32.0763
	L3	8.9775	8.98892	8.93745	8.6528	9.77635	9.39758	8.94416

	Disc	83.2035	83.1944	82.9649	81.8531	86.0921	84.338	83.3047
	ALL	1.46082	0	1.4644	1.44917	1.48216	1.47582	1.4647
	CL	0.010735	0.010751	0.010581	0.011518	0.013768	0.011595	0
LEVEL 3 (L3-L4)	FL	0.966916	1.20353	2.45146	0	1.99722	1.96854	0.730945
	ISL	1.82194	1.78395	1.89993	1.99008	0	2.08854	1.84552
	PLL	0.221103	0.221197	0	0.213372	0.209633	0.220006	0.220255
	SSL	1.24876	1.24075	1.23191	1.40206	1.40781	0	1.26847
	L3	26.6912	26.6987	27.1181	24.7225	20.5928	25.0834	26.46
	L4	31.5758	31.3089	31.3052	34.6469	40.1887	34.2687	32.1011

	Disc	135.464	135.859	135.786	135.618	135.773	135.465	135.544
	ALL	3.3593	3.35736	3.38275	3.36288	3.36341	3.36304	3.36005
	CL	0.016684	0.016627	0.016479	0.016501	0.016602	0.016503	0.016388
LEVEL 4 (L4-L5)	FL	0.569921	0.462519	0.492802	0.430211	0.476465	0.441513	0.404399
	ISL	8.15076	8.24062	8.20315	8.12032	8.21143	8.11862	8.17533
	PLL	0.081633	0.082049	0.079269	0.080714	0.080713	0.081066	0.080601
	SSL	4.89915	4.0282	3.97028	4.84346	4.04438	4.7184	3.87028
	L4	1.36763	1.39	1.42261	1.32906	1.39581	1.4379	1.50297
	L5	20.9238	21.1617	21.1942	20.9374	20.5756	21.0654	20.5215

Results are in N

Table B-8: Transverse Load Forces in Second Axial Rotation

		Control	ALL	PLL	LF	ISL	SSL	CL
	Disc	78.463	77.9945	78.8117	78.6382	78.2515	78.5685	78.8705
	ALL	3.15434	3.09573	3.20827	3.15669	3.11763	3.13349	2.99681
	CL	0.002852	0.002692	0.002915	0.002847	0.002835	0.002757	0.001956
LEVEL 1 (L1-L2)	FL	2.02683	2.00481	2.01693	1.0057	1.01975	2.06504	1.17642
	ISL	0.79362	0.737121	0.822102	0.797214	0.815765	0.766066	0.4216
	PLL	0.151132	0.150752	0.150344	0.150674	0.150812	0.154107	0.151511
	SSL	1.31208	1.09236	1.07794	1.09744	1.12572	1.09574	1.33743
	L1	46.514	46.3878	46.7487	46.6706	46.7687	46.4825	46.6559
	L2	20.6023	20.5439	20.8101	20.7057	20.7708	20.6209	20.1312
	Disc	79.519	79.168	79.6995	78.8753	79.4259	78.8048	79.107
	ALL	2.91637	2.90487	2.93405	2.8973	2.92216	2.88944	2.86899
	CL	0.009127	0.009004	0.009085	0.00918	0.009056	0.00919	0.009451
LEVEL 2 (L2-L3)	FL	0.914768	0.411529	0.060605	0.207957	0.781141	0.208792	0.33025
	ISL	0.809452	0.805118	0.812638	0.752887	0.825848	0.750411	1.08148
	PLL	0.342485	0.3449	0.342575	0.340981	0.339228	0.341023	0.338122
	SSL	0.373497	0.370811	0.356774	0.388391	0.348998	0.39668	0.38029
	L2	24.7517	25.0421	24.4853	24.524	25.16	24.9103	22.2879
	L3	32.692	32.2897	32.4845	33.2514	32.4183	32.9743	29.3937
	Disc	123.834	124.506	123.378	122.762	122.814	122.527	128.312
	ALL	2.73414	0	2.728	2.72417	2.73216	2.72158	2.76115
	CL	0.010229	0.010027	0.01024	0.010305	0.011998	0.011712	0
LEVEL 3 (L3-L4)	FL	0.108714	0.284005	0.45912	0	0.315476	0.155601	0.824784
	ISL	1.54403	1.5667	1.57371	1.4821	0	1.14422	1.79867
	PLL	0.173498	0.180793	0	0.176483	0.192822	0.18502	0.179418
	SSL	0.641684	0.613902	0.641882	0.603902	0.750871	0	0.382986
	L3	26.0385	26.2692	25.8816	26.2936	24.681	25.1277	25.5972
	L4	37.1336	36.0532	36.9889	36.1508	38.0675	38.4583	37.9088
	Disc	162.406	162.093	162.254	161.948	162.364	162.065	156.117
	ALL	1.83143	1.81387	1.84434	1.81286	1.84731	1.79914	1.85821
	CL	0.017502	0.017036	0.017731	0.017251	0.017381	0.017336	0.017495
LEVEL 4 (L4-L5)	FL	0.397832	0.285076	0.542953	0.409807	0.3561	0.355277	0.430197
	ISL	3.19015	3.16025	3.23423	3.18442	3.01467	3.15144	2.80771
	PLL	0.110035	0.107558	0.109975	0.109594	0.109355	0.109793	0.100152
	SSL	2.32187	2.28242	2.4157	2.30645	1.27983	2.2922	1.28383
	L4	32.6335	33.3879	32.1581	32.2209	33.6559	32.3101	33.9314
	L5	12.0413	11.9271	11.2004	11.8968	11.4593	12.1974	14.3484

Results are in N

Table B-9: Transverse Load Forces in Extension

		Control	ALL	PLL	LF	ISL	SSL	CL
	Disc	25.401	28.5988	29.8084	29.2911	29.3254	23.9473	29.53
	ALL	1.05064	1.10613	1.18595	1.16379	1.14633	0.734091	1.05447
	CL	0.002491	0.002452	0.002495	0.002468	0.002531	0.003194	0.002386
LEVEL 1 (L1-L2)	FL	0.059657	0.327437	0.147098	0.47826	0.189461	0.01467	0.331719
	ISL	0.013492	0.001886	0.032293	0.038352	0.048169	0.043598	0.022582
	PLL	0.140821	0.15582	0.151626	0.153811	0.15346	0.180323	0.156508
	SSL	0.003662	0.001093	0.000311	0.000796	0.000508	0.00064	0.000277
	L1	27.1572	25.4356	26.0957	26.1764	25.6562	25.3195	25.9219
	L2	26.0415	26.6789	26.5925	26.3912	26.4281	22.9943	26.7575
	Disc	77.8654	78.1601	81.1083	80.1239	81.1716	79.8045	79.6154
	ALL	1.06881	1.11763	1.08215	1.07699	1.10452	1.15138	1.11089
	CL	0.015186	0.014089	0.014079	0.01267	0.014699	0.016825	0.01604
LEVEL 2 (L2-L3)	FL	0.521341	0.09283	0.129499	0.279379	0.155376	0.38119	0.448546
	ISL	0.294115	0.243047	0.407738	0.259157	0.386744	0.04388	0.200465
	PLL	0.591311	0.587964	0.590043	0.58212	0.587297	0.594022	0.590832
	SSL	0.00032	0.001541	4.84E-05	0.000973	0.000176	0.000351	0.000146
	L2	44.7817	43.8782	44.0517	42.7453	44.781	45.1071	45.0473
	L3	25.0495	26.3577	26.1218	26.6841	26.04	24.7132	24.9252
	Disc	117.287	109.831	104.432	105.98	104.92	109.073	108.482
	ALL	4.00943	0	3.1398	3.28483	3.18599	3.76045	3.58408
	CL	0.018286	0.015696	0.014129	0.014139	0.014391	0.016622	0
LEVEL 3 (L3-L4)	FL	1.10282	0.284621	0.108585	0	0.189301	0.343297	0.444963
	ISL	0.462767	0.584062	0.492013	0.647607	0	0.570441	0.411908
	PLL	0.445532	0.41938	0	0.34706	0.418804	0.415247	0.42171
	SSL	0.000178	0.000239	0.000623	0.00056	0.000309	0	0.000176
	L3	47.3217	46.4251	47.2462	46.5941	47.9972	48.6591	46.9542
	L4	18.9844	18.1454	18.5426	18.6939	18.07	20.7124	18.7012
	Disc	141.555	143.84	143.684	142.651	145.872	146.281	146.602
	ALL	2.73085	2.81505	2.74108	2.75224	2.6816	2.9432	2.91551
	CL	0.014851	0.015243	0.015221	0.014717	0.016874	0.017223	0.015529
LEVEL 4 (L4-L5)	FL	0.199274	0.153974	0.070167	0.094633	0.107269	0.123908	0.126672
	ISL	0.409695	0.48249	0.471977	0.575641	0.5304	0.686454	0.475882
	PLL	0.172299	0.173029	0.171047	0.173773	0.163586	0.170574	0.17533
	SSL	0.000411	0.000414	0.000495	0.000449	0.000311	0.001109	0.000208
	L4	25.9863	26.7771	27.0288	26.6662	25.6161	27.0131	26.7924
	L5	20.9369	21.9178	21.5124	21.2038	22.7322	22.8013	23.7485

Results are in N

Table B-10: Transverse Load Forces in Flexion

		Control	ALL	PLL	LF	ISL	SSL	CL
	Disc	43.3077	43.0783	43.5337	43.2155	43.3966	43.35	43.358
	ALL	0.542863	0.540997	0.534524	0.541621	0.542384	0.544564	0.5429
	CL	0.005654	0.00565	0.005684	0.005649	0.005653	0.005712	0.005722
LEVEL 1 (L1-L2)	FL	6.60355	6.60591	6.63354	6.64072	6.63052	6.69311	6.65453
	ISL	3.04737	3.08234	3.11436	3.08268	3.06285	3.09277	3.04687
	PLL	0.489621	0.484789	0.49215	0.495651	0.499163	0.492919	0.495725
	SSL	1.57066	1.56472	1.57809	1.56712	1.6473	1.57758	1.56641
	L1	5.8381	5.39616	9.07578	4.51186	3.98343	5.94249	3.98916
	L2	2.32032	2.30918	2.55636	2.43517	1.87341	2.35276	2.31552

	Disc	15.4371	15.4657	15.4434	14.9124	15.9264	15.6653	15.4512
	ALL	1.26368	1.2602	1.26048	1.262	1.26475	1.26521	1.26423
	CL	0.006732	0.006724	0.006733	0.006492	0.006625	0.006707	0.006667
LEVEL 2 (L2-L3)	FL	8.15759	8.12407	8.1551	7.9952	8.15603	8.18528	8.13871
	ISL	6.00479	6.02273	6.07461	6.14175	5.95786	6.05252	6.06608
	PLL	0.2112	0.211319	0.210829	0.206211	0.216683	0.211476	0.213058
	SSL	1.58533	1.54056	1.57581	2.05516	1.55647	1.52481	2.02707
	L2	2.57196	2.64736	2.67053	2.67959	2.37728	2.33757	2.3997
	L3	7.38147	7.13074	7.22339	10.5485	5.85825	6.48563	6.93675

	Disc	51.6859	52.0149	52.1707	41.8002	51.4406	50.6129	51.8608
	ALL	1.75205	0	1.75587	1.73996	1.83577	1.81153	1.75646
	CL	0.005691	0.005703	0.005676	0.006626	0.009033	0.00707	0
LEVEL 3 (L3-L4)	FL	13.2359	13.4962	13.1866	0	19.6665	16.3036	14.3822
	ISL	5.16193	5.02595	5.07456	6.88464	0	6.03777	4.75478
	PLL	0.27666	0.273258	0	0.57425	0.403178	0.343438	0.280824
	SSL	1.777	1.72979	1.72468	2.80021	3.16278	0	1.76437
	L3	3.16235	3.35428	3.28903	2.83898	3.01647	3.74931	3.17562
	L4	14.2807	15.0995	14.4159	9.94829	11.4024	13.53	14.3673

	Disc	110.971	110.885	111.031	110.296	111.389	111.553	111.261
	ALL	0.348125	0.349386	0.350808	0.352822	0.346904	0.347116	0.35145
	CL	0.02547	0.025428	0.025486	0.025633	0.02529	0.025384	0.025537
LEVEL 4 (L4-L5)	FL	14.0068	14.0534	14.2124	13.7247	14.0312	14.2946	14.0141
	ISL	3.44517	3.48867	3.53286	3.35249	3.46888	3.55656	3.48254
	PLL	0.037292	0.039383	0.037413	0.036093	0.038618	0.039223	0.035772
	SSL	4.04236	4.03082	4.04514	4.04385	4.05293	4.03238	4.05168
	L4	1.64629	1.60191	1.57595	1.34711	1.65551	1.77868	1.60205
	L5	8.66303	8.53661	8.81219	8.46213	8.83065	8.82229	8.70681

Results are in N

Table B-11: Transverse Load Forces in First Lateral Bending

		Control	ALL	PLL	LF	ISL	SSL	CL
	Disc	19.3713	19.4116	19.4606	18.6004	19.161	19.5627	19.7301
	ALL	0.675525	0.684217	0.681376	0.704915	0.679079	0.67811	0.657701
	CL	0.004771	0.004774	0.004844	0.00484	0.004893	0.004813	0.004744
LEVEL 1 (L1-L2)	FL	4.44546	4.53446	4.7085	4.68153	4.57404	4.4807	4.39356
	ISL	0.427455	0.431869	0.441711	0.415784	0.423246	0.454809	0.420784
	PLL	0.264591	0.265698	0.267453	0.266899	0.265862	0.262568	0.262534
	SSL	0.683889	0.869089	0.701117	0.851911	0.705913	0.712304	0.666705
	L1	30.2427	30.7038	30.0348	29.909	30.0971	30.7265	30.22
	L2	22.5925	22.5516	22.7105	22.7339	22.598	22.8086	22.7357

	Disc	4.27795	5.50835	4.65654	5.15953	4.48137	5.45736	6.62118
	ALL	0.57608	0.612582	0.587598	0.610152	0.586255	0.587258	0.640263
	CL	0.012298	0.012218	0.012375	0.012224	0.012348	0.012334	0.012389
LEVEL 2 (L2-L3)	FL	5.3483	5.45486	5.32316	5.31512	5.28831	5.49369	5.48809
	ISL	0.297621	0.41261	0.339858	0.284995	0.392366	0.368365	0.410616
	PLL	0.061515	0.05652	0.062679	0.066389	0.061691	0.063312	0.065118
	SSL	0.540206	0.632298	0.524623	0.615183	0.591116	0.555077	0.526812
	L2	16.6508	16.5399	16.7241	16.3769	16.8132	17.5146	17.8128
	L3	12.1082	15.7968	11.9987	11.7195	11.7329	13.0752	12.7201

	Disc	49.2228	49.7854	48.8881	39.5834	46.6715	47.9519	49.3343
	ALL	1.60524	0	1.62043	1.62334	1.60529	1.62273	1.59101
	CL	0.013266	0.014504	0.013071	0.012139	0.013416	0.013111	0
LEVEL 3 (L3-L4)	FL	5.96521	6.44223	5.86933	0	6.67832	6.01061	5.33803
	ISL	1.57139	1.4632	1.58747	2.53576	0	1.71341	1.60567
	PLL	0.557849	0.530784	0	0.7174	0.60815	0.568284	0.560129
	SSL	0.895254	0.875162	0.894066	1.00711	0.9268	0	0.891989
	L3	19	17.8845	18.9899	15.6218	16.4876	17.9772	20.0162
	L4	7.58321	4.96995	7.59815	8.74479	7.55376	7.00356	8.74902

	Disc	113.679	113.509	113.407	113.146	113.345	113.667	113.335
	ALL	0.933598	0.947201	0.976792	0.962965	0.939446	0.919012	0.961027
	CL	0.008651	0.0085	0.008679	0.008675	0.008644	0.008498	0.008706
LEVEL 4 (L4-L5)	FL	4.07737	4.44827	4.17457	3.81679	3.95491	4.30337	3.97063
	ISL	1.62795	1.67902	1.61829	1.6327	1.56448	1.60246	1.72953
	PLL	0.112001	0.120674	0.111723	0.110731	0.104748	0.112893	0.116803
	SSL	1.52211	1.49527	2.42837	2.46499	2.38949	1.52268	1.54571
	L4	3.39453	2.9052	3.14554	3.4407	3.56628	3.5653	3.51882
	L5	10.5221	11.1343	11.242	10.5486	10.7859	10.1027	10.3133

Results are in N

Table B-12: Transverse Load Forces in Second Lateral Bending

		Control	ALL	PLL	LF	ISL	SSL	CL
	Disc	22.2355	22.5912	22.4575	22.4677	22.1917	22.4442	22.5172
	ALL	2.8404	2.84165	2.84427	2.84274	2.84017	2.84273	2.83868
	CL	0.00249	0.002478	0.002481	0.002468	0.002466	0.002475	0.002477
LEVEL 1 (L1-L2)	FL	0.898808	0.941219	0.932647	0.93717	0.929947	0.939232	0.932564
	ISL	0.472294	0.474621	0.464437	0.46869	0.464752	0.468673	0.481938
	PLL	0.220369	0.222584	0.22218	0.222905	0.219429	0.222482	0.222651
	SSL	0.340742	0.452315	0.34397	0.344748	0.339469	0.457721	0.344742
	L1	11.7289	11.812	11.7788	11.763	11.7857	11.7836	11.7875
	L2	7.13581	7.32428	7.19978	7.18594	7.20192	7.1777	7.23541
	Disc	19.9077	20.0873	20.0317	19.7699	19.4636	19.5549	19.8513
	ALL	1.98492	1.98149	1.97569	1.9843	1.98984	1.98539	1.98635
	CL	0.008853	0.008862	0.008885	0.008837	0.005986	0.006015	0.005975
LEVEL 2 (L2-L3)	FL	1.38458	1.04761	1.2028	1.02756	1.20155	1.16152	1.21228
	ISL	0.691992	0.669031	0.71359	0.709236	0.666489	0.702939	0.696017
	PLL	0.295684	0.295502	0.295045	0.295367	0.296687	0.29389	0.297232
	SSL	0.402932	0.473066	0.472847	0.407277	0.396071	0.409613	0.401379
	L2	4.89425	5.12233	4.9188	4.95805	4.94818	4.90772	5.0593
	L3	5.78699	6.01029	5.82864	5.38932	6.06897	6.02886	5.88129
	Disc	56.8185	57.8994	56.8656	54.8767	54.2643	54.785	57.0328
	ALL	2.42106	0	2.4111	2.42566	2.43356	2.41642	2.43338
	CL	0.015207	0.015407	0.015177	0.015429	0.016201	0.015472	0
LEVEL 3 (L3-L4)	FL	0.462251	0.601927	0.578491	0	1.26544	1.2404	0.927035
	ISL	1.29817	1.2653	1.26244	1.39166	0	1.49497	1.28599
	PLL	0.226209	0.215754	0	0.239224	0.254781	0.242702	0.222618
	SSL	0.980733	0.815156	0.970463	1.07552	1.0309	0	0.818743
	L3	21.3538	22.0679	21.2566	21.1922	20.9805	20.4986	21.419
	L4	25.7808	26.5447	25.827	25.4213	23.8089	24.8667	26.1248
	Disc	106.131	105.698	105.901	105.786	106.091	105.95	105.926
	ALL	2.49632	2.48619	2.48878	2.48129	2.47524	2.47411	2.48188
	CL	0.003766	0.003672	0.00375	0.003683	0.00369	0.003706	0.00374
LEVEL 4 (L4-L5)	FL	0.960577	1.00891	0.983976	0.983283	0.989486	1.01001	1.00417
	ISL	1.65203	1.65352	1.65685	1.64803	1.62771	1.63745	1.6606
	PLL	0.048357	0.048422	0.048389	0.048207	0.047983	0.048146	0.048304
	SSL	0.853833	0.877869	0.868362	0.869632	1.1497	1.17343	0.883108
	L4	2.08981	2.01133	2.06001	1.98018	2.13261	2.06303	2.03442
	L5	6.33161	6.72562	6.39764	6.45623	6.68026	6.48982	6.23605

Results are in N

APPENDIX C. LOADING FILES

The following sections demonstrate some of the materials and loading files that were used in the file. They are coded in LS-Dyna format, but can be interpreted or adapted in to other program files with help of the LS-Dyna KEYWORD User's Manual [51].

C.1 Loading

Initial Loading for Compression

```
*KEYWORD
*TITLE
Compression
*CONTROL_PARALLEL
2,0,0,0
*CONTROL_TERMINATION
30
*CONTROL_TIMESTEP
,0.8,,,-6.0e-7
*CONTROL_ENERGY
2
*CONTROL_CONTACT
,,2

*CONTROL_SHELL

,1,
*DATABASE_EXTENT_BINARY
,,,1

$
$
*DAMPING_GLOBAL
0,2
*DATABASE_BINARY_D3PLOT
30
*DATABASE_RCFORC
0.002
$*DATABASE_BINARY_INTFORC
$0.002
```

```
$
*INCLUDE
matsSTempF.k
*INCLUDE
Control.k
*INCLUDE
tempsF.k
*CONTACT_SURFACE_TO_SURFACE
1,2,0,0,,,0,0
0.000,0.000,0.000,0.000,0.000,0,0.000,0.000

*CONTACT_NODES_TO_SURFACE
111,4,4,0,,,0,0
0.000,0.0000,0.000,0.000,0.000,0,0.000,0.000
.05,1,,,1,1,1,1
*CONTACT_SURFACE_TO_SURFACE
5,6,0,0,,,0,0
0.000,0.000,0.000,0.000,0.000,0,0.000,0.000

*CONTACT_SURFACE_TO_SURFACE
7,8,0,0,,,0,0
0.000,0.000,0.000,0.000,0.000,0,0.000,0.000

*CONTACT_SURFACE_TO_SURFACE
9,10,0,0,,,0,0
0.000,0.000,0.000,0.000,0.000,0,0.000,0.000

*CONTACT_SURFACE_TO_SURFACE
11,12,0,0,,,0,0
0.000,0.000,0.000,0.000,0.000,0,0.000,0.000

$*CONTACT_TIEBREAK_SURFACE_TO_SURFACE
$3,4,0,0,,,0,0
$0.000,0.000,0.000,0.000,0.000,0,0.000,0.000
$0,0,0,0
```

Code Added for Loading after Compression

```
*KEYWORD
*CONTROL_TERMINATION
320
*DAMPING_GLOBAL
0,.19
*DATABASE_BINARY_D3PLOT
1
*CHANGE_CURVE_DEFINITION
1
*DEFINE_CURVE
1
0,0
30,0
300,-8000
*END
```

C.2 Materials

C.2.1 Rigid Bodies

```
*MAT_RIGID
1,1.9130E-03,999.7398,0.200,,,
0,0,0
0
*DEFINE_COORDINATE_SYSTEM
1,0.004,-16.536,0.065,1.00339,-16.536,0.1
0.004,-15.5366,0.1
*HOURGLASS
1,1,0.0,0,0.0,0.0
*SECTION_SHELL
1,1,0.0,3.0,0.0,0.0,0
0.25,0.25,0.25,0.25,0.0
*PART
T12 Interface
1,1,1,0,1,0,0,0
```

C.2.2 Vertebrae

```
*MAT_TEMPERATURE_DEPENDENT_ORTHOTROPIC
2,1.8745E-03,2
,,,1,0,0
,,,1,1,0
691.19,471.36,1645.03,0.23,0.40,0.38
0.00,0.00,0.00,251.53,301.84,215.60,-1000
691.19,471.36,1645.03,0.23,0.40,0.38
0.00,0.00,0.00,251.53,301.84,215.60,74.999
68.97,47.04,164.16,0.226,0.399,0.381
0,0,0,25.1,30.12,21.51,75
4972.03,3390.67,11833.44,0.23,0.40,0.38
0.00,0.00,0.00,1809.39,2171.27,1550.91,5000
*HOURGLASS
2,1,0.0,0,0.0,0.0
*SECTION_SOLID
2,1,0,0
*PART
L1 Vertebra
2,2,2,0,2,0,0,0

*MAT_ELASTIC
69,1.914E-03,12000.0,0.2,,,
*HOURGLASS
69,1,0.0,0,0.0,0.0
*SECTION_SHELL
69,1,0.0,3.0,0.0,0.0,0
0.4,0.4,0.4,0.4,0.0
*PART
Cortical Bone
69,69,69,0,69,0,0,0
```

C.2.3 Intervertebral Discs

```
*MAT_MOONEY-RIVLIN_RUBBER
8,1.0003E-03,.49,.5,.05

*HOURGLASS
8,6,1.0,0,0.0,0.0
*SECTION_SOLID
8,1,0
*PART
Nucleus Pulposus T12-L1
8,8,8,0,8,0,0,0

*MAT_ORTHOTROPIC_ELASTIC
9,1.0003E-03,5.5999,0.3400,0.1900,0.107,0.0112,0.0782
0.1000,0.1000,0.1000,4.0,6.894E-007
17.5257,98.359,234.046
0.1541,-0.3886,0.8310
*HOURGLASS
9,6,1.0,0,0.0,0.0
*SECTION_SOLID
9,1,0
*PART
Inner AF T12-L1

*MAT_ORTHOTROPIC_ELASTIC
10,1.0003E-03,17.4575,0.2700,0.1900,0.0274,0.0036,0.00152
0.1000,0.1000,0.1000,4.0,6.894E-007
17.5257,98.359,234.046
0.1541,-0.3886,0.8310
*HOURGLASS
10,6,1.0,0,0.0,0.0
*SECTION_SOLID
10,1,0
*PART
Outer AF T12-L1
10,10,10,0,10,0,0,0
```

C.2.4 Ligaments

```
*MAT_FABRIC
26,1.0003E-03,2,2,2,0.3,0.3,0.3
0.0,0.0,0.0,1.0,0.0,0.0,0.0,0.5
0.0,0.0,0.0,0.0,0.0,4
0.0,0.0,0.0,0.0,0.0,0.0
0.0,0.0,0.0,0.0,0.0,0.0
26
*HOURGLASS
26,0,0.0,0,0.0,0.0
*SECTION_SHELL
26,1,0.0,3.0,0.0,0.0,1
```

```
0.9398,0.9398,0.9398,0.9398,0.0
0,90,0
*PART
ALL
26,26,26,0,26,0,0,0
*DEFINE_CURVE
26,0,0.0,0.0,0.0,0.0,0
0.0,0.0
0.12,1.15
0.44,9.11
0.57,10.3
```

C.2.5 Follower Load

```
*MAT_ELASTIC_SPRING_DISCRETE_BEAM
35,0.002,.001,444

*HOURGLASS
35,1,0.0,0,0.0,0.0
*SECTION_BEAM
35,6

*PART
FOLLOWER
35,35,35,0,35,0,0,0
```

C.3 Supercomputer

Compression Loading

```
#!/bin/bash

#PBS -l nodes=1:ppn=12,mem=16gb,walltime=35:00:00
#PBS -N ConFLEX
#PBS -m bea
#PBS -M gfun4all@gmail.com

# Set the max number of threads to use for programs using OpenMP. Should be
<= ppn. Does nothing if the program doesn't use OpenMP.
export OMP_NUM_THREADS=12
export LSTC_LICENSE=network
export LSTC_LICENSE_SERVER=fsllinuxlic4
export LSTC_LICENSE_SERVER_PORT=13373

# The following line changes to the directory that you submit your job from
cd "$PBS_O_WORKDIR"

/fslhome/fun4all/fsl_groups/fslg_babel/lsdyna/ls971d i=loadingSTempF.k
memory=1000m

exit 0
```

Loading Cases

```
#!/bin/bash

#PBS -l nodes=1:ppn=2,mem=9gb,walltime=300:00:00
#PBS -N 3f
#PBS -m bea
#PBS -M gfun4all@gmail.com

# Set the max number of threads to use for programs using OpenMP. Should be
<= ppn. Does nothing if the program doesn't use OpenMP.
export OMP_NUM_THREADS=12
export LSTC_LICENSE=network
export LSTC_LICENSE_SERVER=fsllinuxlic4
export LSTC_LICENSE_SERVER_PORT=13373

# The following line changes to the directory that you submit your job from
cd "$PBS_O_WORKDIR"

/fslhome/fun4all/fsl_groups/fslg_babel/lsdyna/ls971d r=d3dump01 i=add.k
memory=1000m

exit 0
```